Advanced photocatalysis mediated by TiO_2/Ag/TiO_2 nanoparticles modified cotton fabric

Milica Milošević [a], Marija Radoičić [a,*], Satoshi Ohara [b], Hiroya Abe [b], Jelena Spasojević [a], Lidija Mančić [c], Zoran Šaponjić [d]

[a] University of Belgrade, Vinča Institute of Nuclear Sciences - National Institute of the Republic of Serbia, Mike Petrovića Alasa 12 - 14, 11351 Vinča, Belgrade, Serbia.

[b] Joining and Welding Research Institute, Osaka University, Mihogaoka 11 - 1, Ibaraki, Osaka 567 - 0047, Japan.

[c] Institute of Technical Sciences of the Serbian Academy of Sciences and Arts, Kneza Mihaila 35, 11000 Belgrade, Serbia.

[d] Institute of General and Physical Chemistry, Studentski trg 12/V, 11158 Belgrade, Serbia.

[*] Corresponding author: Marija Radoičić, University of Belgrade, Vinča Institute of Nuclear Sciences - National Institute of the Republic of Serbia, Mike Petrovića Alasa 12 - 14, 11351 Vinča, Belgrade, Serbia.
E-mail address: mradoicic@vin.bg.ac.rs.

The author's e-mail addresses:

Milica Milošević: milicam@vin.bg.ac.rs
Satoshi Ohara: ohara@jwri.osaka-u.ac.jp
Hiroya Abe: h-abe@jwri.osaka-u.ac.jp
Jelena Spasojević: jelenas@vin.bg.ac.rs
Lidija Mančić: lidija.mancic@itn.sanu.ac.rs
Zoran Šaponjić: zsaponjic@iofh.bg.ac.rs

Abstract

Novel cotton-based $TiO_2/Ag/TiO_2$ nanocomposites for wastewater treatment were developed by fine chemical synthesis path with the goal of coping with wastewater issues and environmental remediation. The photocatalytic performances of nanocomposites were tested during photodegradation processes of RB, AO7 and MR under simulated solar light. Double- and single-loaded nanocomposites were synthesized by a simple bottom-up approach implying *in situ* photoreduction of Ag^+ ions on the surface of TiO_2 NPs previously deposited on cotton fibers from colloids.

The spherical-like colloidal TiO_2 NPs (4.5 nm) and TiO_2/Ag NPs (8 nm) and the formation of uniform TiO_2/Ag and $TiO_2/Ag/TiO_2$ nano-coatings on cotton fibers were examined by TEM and FESEM. The reduction of Ag^+ ions on TiO_2 surface was undoubtedly proven by the appearance of SPR band of Ag NPs in UV/Vis spectra. Raman spectroscopy clearly confirmed the presence of anatase TiO_2 in nanocomposites. Quantitative determination of TiO_2 and Ag in nanocomposites was accomplished using EDX and ICP – OES.

The cotton-based $TiO_2/Ag/TiO_2$ nanocomposite showed the highest photocatalytic efficiency (> 90%) and maintained its removal efficiency after three reuse cycles, indicated its exceptional photochemical ability. The initial idea of improved photocatalytic performances of a TiO_2 NPs double-layer with immobilized Ag NPs was justified as the $TiO_2/Ag/TiO_2$ processed sample contributed additional binding sites for dye molecules. Considering that the photocatalytic activity of the cotton-based TiO_2 and TiO_2/Ag samples was practically imperceptible, it can be assumed that the synthesized Ag NPs act predominantly as electron traps in the double-loaded synthesized system.

Abbreviation

NPs - nanoparticles
CO control - control cotton fabric
CO+TiO_2 - TiO_2 NPs modified cotton fabric sample
CO+TiO_2/Ag - TiO_2/Ag NPs modified cotton fabric composite
CO+$TiO_2/Ag/TiO_2$ - $TiO_2/Ag/TiO_2$ NPs modified cotton fabric composite
RB - Rhodamine B
AO7 - Acid Orange 7
MR - Methyl Red
TEM - Transmission Electron Microscopy
FESEM - Field Emission Scanning Electron Microscopy
EDX - Energy Dispersive X-ray Spectroscopy
ICP – OES - Inductively Coupled Plasma - Optical Emission Spectroscopy
UV/Vis – Ultraviolet/Visible Spectroscopy
DRS – Defuse Reflectance Spectra

81   AOPs - advanced oxidation processes
82   PD - photocatalytic degradation
83   C_0 - the initial concentration of the dye solution (*zero point*)
84   C - concentration of the dye solution in the selected illumination time interval
85   CB - conduction band
86   VB - valence band
87   E_f – Energy of Fermi level
88   E_{SPR} – Energy of surface plasmon resonance
89   e^- - electrons
90   h^+ - holes
91   SPR - surface plasmon resonance
92   Xe – xenon
93
94

95   *1. Introduction*
96

97   The current emphasis on environmental safety and wastewater issues raises increasing
98 awareness and demands for the treating of residual water polluted by various dyes (e.g. from the
99 textile, paper, cosmetic and pharmaceutical industries). In addition to the significant influence,
100 especially of textile dyes, on the aesthetic quality of water bodies, there is also an increase in the
101 biochemical and chemical oxygen demand, undermining photosynthesis, provoking serious
102 problems for plant and aquatic life as well as to human health disorders that cause toxicity,
103 mutagenicity and carcinogenicity (Khataee and Kasiri 2010; Lellis *et al.* 2019). The significant
104 importance of these concerns gave rise to strict mandates respecting wastewater issues related to
105 their treatment technologies, including AOPs (Khataee and Kasiri 2010; Julkapli *et al.* 2014;
106 Anwer *et al.* 2019; Yaseen and Scholz 2019).

107   The AOPs appear to be one of the most effective processes for treating organic pollutants in
108 wastewater (Khataee and Kasiri 2010; Ghime and Ghosh 2020). Among AOPs, heterogeneous
109 photocatalysis using TiO_2 nanocrystals has undoubtedly become one of the most frequently used
110 system for the dye degradation treatment, due to the simple synthesis of TiO_2 NPs, their low cost,
111 photostability, photocorrosion resistance and non-toxic and inert nature. In general, bare
112 semiconductive TiO_2 nanomaterials (without doping and structural modification) are capable of
113 decomposing organic compounds into their simpler forms and/or mineralize them to CO_2 and H_2O
114 but only under the UV part of sunlight irradiation. Interest in tailoring the optical properties of
115 TiO_2 by doping with impurity elements (metal/nonmetal) in order to improve its photosensitivity
116 and photocatalytic activity in the visible wavelength range has not diminished recently
117 (Kapilashrami *et al.* 2014). On the other hand, there is another way to improve its photocatalytic
118 efficiency which implies loading the TiO_2 systems with a noble metal. This approach is based on
119 the fact that the E_f of noble metals is usually lower than the energy of CB of the TiO_2
120 semiconductor (Linsebigler *et al.* 1995; Kamat 2002; Chiarello *et al.* 2010). Thus, photogenerated

121 e⁻ from the CB of TiO$_2$ can migrate and be captured by the noble metal. At the same time,
122 photogenerated h$^+$ in the VB of TiO$_2$ are available to participate in oxidative photocatalytic
123 degradation processes. In general, the recombination of photogenerated charges in TiO$_2$ is
124 suppressed in this way, which enables a higher photocatalytic efficiency of TiO$_2$.

125 The target spot in the photodegradation processes is the dye chromophore, as it represents the
126 part of the molecule (an unsaturated group, e.g. azo, keto, nitro) where absorption proceeds and
127 where excitation causes major changes in geometry or electron density of the molecule
128 (Chakraborty 2014; Kuball *et al.* 2017). Based on the chromophore structure, synthetic dyes are
129 classified into reactive, basic, direct, solvent and vat dyes and divided into subcategories: thiazine,
130 xanthene, azo, anthraquinone and triarylmethane, among others (Anwer *et al.* 2019). RB, a basic
131 cationic dye, is the most dominant colorant in the xanthene group of dyes, while AO7 and MR
132 belong to anionic monoazo acid dyes.

133 The preparation of surface-modified textile fabrics with various types of metal-oxides and
134 metal NPs, primarily in the last two decades, has opened up the possibility for manufacturing so-
135 called high-added-value textile products. Such a technological approach encounters plentiful
136 obstacles related to the method of synthesis, the deposition procedure and the concentration of the
137 used metal and/or metal-oxide NPs. Therefore, there is still a plenty of room for improvement the
138 efficiency and stability of such textile-based nanocomposite materials.

139 The mechanical, chemical, photochemical and thermal stability of textile materials made
140 these materials adequate support for composite particles. Multifunctionality and far-reaching use
141 of the resulting textile nanocomposites (self-cleaning, antimicrobial activity, UV protection,
142 superhydrophilicity/superhydrophobicity, etc.) is extensively recognized (Morones *et al.* 2005;
143 Zhang *et al.* 2007; Dastjerdi and Montazer 2010; Montazer *et al.* 2011; Mihailović *et al.* 2011;
144 Radetić 2013a, b; Rivero *et al.* 2015; Milošević *et al.* 2017) and their potential was used within
145 this research.

146 In our previous work, we engineered a multifunctional textile nanocomposite material based
147 on polyester fabric modified with separately synthesized sequentially deposited Ag and TiO$_2$ NPs.
148 This study revealed that the presence of Ag NPs considerably affects the antimicrobial efficiency
149 and photodegradation activity of TiO$_2$ (Mihailović *et al.* 2011).

150 The topic of this study was advanced photocatalysis mediated by composite TiO$_2$/Ag/TiO$_2$ NPs
151 deposited on cotton fabric, including bottom-up synthesis, detailed structural, optical and
152 morphological characterization in addition to examination its photocatalytic efficiency and
153 reusability in the process of textile dyes decomposition (RB, AO7 and MR). The bottom-up
154 synthesis approach implied *in situ* photoreduction of Ag$^+$ ions on the surface of TiO$_2$ NPs
155 previously deposited from a colloidal dispersion to the surface of cotton fibers. Immobilized Ag
156 NPs, which behave as electron scavengers, can enhance the photocatalytic efficiency of TiO$_2$ NPs.
157 The photocatalytic efficiency was tested as a function of the amounts of Ag and TiO$_2$ NPs and
158 their order of deposition as well as a function of the stability of such a textile-based nanocomposite

159 system. To the best of our knowledge, the synthesis of cotton fabric modified with composite
160 $TiO_2/Ag/TiO_2$ NPs in the proposed manner was performed here for the first time.
161
162   *2. Experimental*
163
164   *2.1. Textile material*
165
166   The cotton woven fabric (desized & bleached, 117.5 g/m^2, 27 ends/cm, 52 picks/cm,
167 thickness of 0.26 mm) was used as undercoat within this research. The fabric was cleaned of
168 surface impurities before finishing with TiO_2/Ag NPs as described elsewhere (Milošević *et al.*
169 2013). The control sample (CO control), used in this research, refers to a cotton fabric sample.
170
171   *2.2. Synthesis of nanocomposite textile materials (photocatalysts)*
172
173   Synthesis of photocatalysts, including TiO_2 NPs modified cotton fabric sample (CO+TiO_2),
174 TiO_2/Ag NPs modified cotton fabric composite (CO+TiO_2/Ag) and $TiO_2/Ag/TiO_2$ NPs modified
175 cotton fabric composite (CO+$TiO_2/Ag/TiO_2$), was carried out using a simple bottom-up approach
176 through the following steps:

177   1) Synthesis of TiO_2 NPs.
178   2) Finishing of cotton fabric with TiO_2 NPs by dip-coating method.
179   3) *In situ* synthesis of Ag NPs on the surface of TiO_2 NPs previously deposited on cotton
180   fabric from colloids.
181   4) Formation of $TiO_2/Ag/TiO_2$ sandwich nanostructure.

182   In that manner, the following materials were synthesized through specified steps: CO+TiO_2
183 (*steps 1 and 2*), CO+TiO_2/Ag (*steps 1, 2 and 3*) and CO+$TiO_2/Ag/TiO_2$ (*steps 1, 2, 3 and 4*).

184   All chemicals used for synthesis were commercial analytical quality products (*J. T. Baker*,
185 *Fluka*, *Kemika*, *Reanal* – specified in the *Supplementary Information*) and were used as received
186 without any further purification. *Milli-Q* deionized water was used as a solvent.
187
188   *2.2.1. Synthesis of colloidal TiO_2 NPs*
189
190   A brief overview of the two-step synthesis implied: 1) dropwise addition of cooled $TiCl_4$ to
191 cooled water and dialysis against water until the pH of the solution reached 3.5, thereby achieving
192 the formation and slow growth of amorphous TiO_2 NPs (d ~ 4.5) (Rajh *et al.* 1998) and 2) thermal
193 treatment in reflux (60 °C, 16 h), which manages the amorphous-to-crystalline transformation of
194 anatase and consequently enhances the potential photocatalytic efficiency of the generated NPs (d
195 ~ 6 nm). The particles obtained in this manner were used in all further synthesis routes. A synthesis
196 setup for TiO_2 NPs is described in detail in the aforementioned literature (Rajh *et al.* 1998).
197

2.2.2. Synthesis of colloidal TiO$_2$/Ag NPs

199

200   In order to monitor and evaluate the photoreduction efficiency of Ag$^+$ ions on the surface of
201 TiO$_2$ NPs and the formation of TiO$_2$/Ag NPs in the liquid phase, the prepared reaction system was
202 illuminated with a xenon (Xe) lamp and the UV spectra of the obtained dispersion were recorded
203 at a precisely defined illumination time. Namely, the reaction mixture (15 ml) was gained by
204 mixing the following solutions: 1) alanine (1.5×10^{-2} M), 2) colloidal TiO$_2$ dispersion in HNO$_3$ (7
205 $\times 10^{-3}$ M), 3) AgNO$_3$ (4.5×10^{-3} M) and 4) CH$_3$OH (0.1 M). The prepared system was transferred
206 to a quartz vessel, closed with a rubber septum and bubbled in a argon stream for 20 min.
207 Thereafter, the solution was illuminated with a Xe lamp while taking aliquots at certain time
208 intervals (0, 60 min, 70 min, 90 min, 105 min, 135 min). The optical properties were monitored
209 by measuring the absorption spectra and the illumination was performed until the complete
210 reduction of Ag$^+$ ions, wich is justified in the absorption spectra.

211

212   *2.2.3. Finishing of cotton fabric with TiO$_2$ NPs*

213

214   Finishing of cotton fabric with TiO$_2$ NPs was fulfilled by dip-coating method according to a
215 modified synthesis procedure used in our previous study (Milošević *et al.* 2014). Namely, 1.0 g of
216 cotton fabric was immersed into 30 mL of 0.1 M colloidal TiO$_2$ dispersion for 5 min. After drying
217 in an oven (40 °C), the sample was rinsed twice (5 min) with distilled water. Subsequently, the
218 fabric was dried again at the same temperature.

219

220   *2.2.4. Photoinduced in situ synthesis of Ag NPs onto TiO$_2$ NPs single-layer modified cotton*
221   *surface*

222

223   The Ag NPs were synthesized by *in situ* photoreduction of Ag$^+$ ions on the surface of TiO$_2$
224 NPs previously deposited on cotton fabric in a similar manner as in our earlier research (Milošević
225 *et al.* 2013, 2014). In the course of photoreduction, an ULTRA-VITALUX lamp (300 W, *Osram*)
226 was used, which simulates sun-like irradiation, with a spectral radiation power distribution
227 between 300 and 1700 nm (photometrical data: UVB 280-315 nm 3.0 W, UVA 315-400 nm 13.6
228 W, while the rest is visible and infrared light).

229   The cotton fabric modified with TiO$_2$ NPs (1.0 g) was immersed in a alanine solution (0.1333
230 g / 40 mL H$_2$O) for 10 min. On the other hand, a solution containing HNO$_3$ (58 mL, pH 3), AgNO$_3$
231 (0.015 M, 150 μL) and CH$_3$OH (0.4 mL) was assembled. The prepared solution is added to the
232 alanine solution with the immersed fabric and mixed. The glass vessel was covered with a quartz
233 glass disc and sealed with parafilm. Through a teflon hose inserted into the glass, the system is
234 saturated with argon stream for 20 min and subsequently illuminated for 10 min. The distance
235 between the lamp and the sample was set at 26 cm. After illumination, the fabric was dried at room
236 temperature, rinsed with distilled water (900 mL, 15 min) and likewise dried at room temperature.

237 Argon (*Messer Tehnogas*), used to remove oxygen during the photoreduction process, was of high
238 purity (99.5%).

239
240 *2.2.5. Double-layer deposition of TiO₂ NPs onto previously synthesized TiO₂/Ag*
241 *nanocomposite modified cotton surface*

242
243 The fresh finishing of the cotton fabric with TiO_2 NPs was carried out by dip-coating method.
244 0.5 g of cotton fabric modified with TiO_2/Ag NPs was immersed into 0.1 M TiO_2 colloidal solution
245 (15 mL) for 5 min. Thereafter, the sample was dried in an oven (40 °C), subsequently rinsed twice
246 (5 min) with distilled water and dried again in the oven (40 °C).

247
248 *2.3. Methods*

249
250 *2.3.1. TEM analysis*

251
252 The shape and size of the synthesized colloidal TiO_2 and TiO_2/Ag NPs were determined by
253 TEM using a *JEOL 100CX* device operating at 100 kV.

254
255 *2.3.2. FESEM and EDX analyses*

256
257 The surface morphology of the cotton fabric, previously and after nanofinishing with
258 TiO_2/Ag NPs, was examined using Field Emission Scanning Electron Microscopy (FESEM,
259 *Hitachi SU-70*) operating at 5 kV. The samples were fixed on an Al holder with C tapes and coated
260 with a thin film of Au/Pd (85/15) prior to the analysis. In order to examine the surface elemental
261 composition of nanocomposite textile materials, Energy Dispersive X-ray Spectroscopy (EDX,
262 *Oxford Instruments*) was applied. The EDX analysis was carried out by the FESEM and operated
263 at 15 kV. Fixed samples on an Al holder using C tapes were coated with a thin layer of C before
264 analysis. Treatment options were as follows: all elements were analysed (normalized), repeat times
265 = 3; standard: C ($CaCO_3$), 1999/06/01, O (SiO_2) 1999/06/01, Ti (Ti) 1999/06/01, Ag (Ag)
266 1999/06/01.

267
268 *2.3.3. Raman analysis*

269
270 The structural fingerprint of TiO_2 was provided by Raman analyses. Raman spectra excited
271 by a diode-pumped solid-state laser (at an excitation wavelength and filter of 532 nm and laser
272 power level of 10.0 mW) were collected on a *Thermo Scientific DXR Raman Microscope* equipped
273 with a research optical microscope and a CCD detector. The laser beam was focused onto the
274 sample placed on a X-Y motorized sample stage using a 10× objective magnification. The scattered
275 light was analyzed by a spectrograph with a grating of 900 lines/mm. The exposure time was 30 s

276 with a number of exposures of 10. The instrument aperture was a 50 μm pinhole. The fluorescence
277 correction was estimated by a polynomial fitting order of 5.

278
279 *2.3.4. XRD analyses*
280
281 The crystallographic structure of samples (CO, CO+TiO$_2$/Ag/TiO$_2$) was acquired by X-ray
282 powder diffraction (XRD) measurements using a Philips PW 1050 diffractometer with Ni-filtered
283 Cu-K$_\lambda$ radiation ($\lambda = 1.5418$ Å). The diffraction intensity was measured by the scanning technique
284 (a step size of 0.05° and a counting time of 50 s per step).

285
286 *2.3.5. ICP - OES analysis*
287
288 The total content of deposited Ti and Ag on the examined samples was determined by
289 Inductively Coupled Plasma - Optical Emission Spectroscopy (ICP - OES) with a *Thermo*
290 *Scientific ICAP 7600* instrument. A sample (0.04 g) was immersed in concentrated H$_2$SO$_4$ (60 mL)
291 and heated moderately to 60 °C. In the case of the CO+TiO$_2$ sample, complete fabric degradation
292 was followed by total carbonization after 45 min. Otherwise, in respect of CO+TiO$_2$/Ag and
293 CO+TiO$_2$/Ag/TiO$_2$ fabrics, 2 mL of HNO$_3$ (1:1) was subsequently added and a clear homogenous
294 solution was obtained after a total of 30 min. All samples were diluted 10× prior to the analysis.

295
296 *2.3.6. UV/Vis analysis*
297
298 The absorption intensities of the dyes for the photocatalytic activity test measurements are
299 examined using a UV/Vis with a *Thermo Scientific Evolution 600* UV/Vis spectrophotometer. The
300 reference dyes intensities were as follows: $\lambda_{max} = 554$ nm (RB), $\lambda_{max} = 485$ nm (AO7) and $\lambda_{max} =$
301 520 nm (MR). The same device was used to monitor the absorption properties of the TiO$_2$/Ag NPs
302 colloidal dispersion for different illumination times.

303 The deposition of Ag NPs on the surface of the nanocomposite samples was followed by
304 UV/Vis reflectance analysis. Reflectance spectra were obtained with a *Datacolor Spectralflash SF*
305 *300* spectrophotometer under illuminant D$_{65}$ using a standard 10° observer.

306
307 *2.3.7. Photocatalytic activity test*
308
309 The photocatalytic performances of the synthesized samples were examined by following the
310 degradation capacity of the test dye molecules under simulated solar light: RB, AO7 and MR. The
311 photodegradation of the investigated dyes is monitored by the concentration changes (C/C$_0$) of
312 dyes as a function of the illumination time. Aqueous solutions of 10 mg/L of RB and AO7 were
313 prepared at 25 °C with short-time stirring, while the same concentration of MR was prearranged
314 in HCl (1 mol/L, 50 mL) with continuous stirring at 60 °C for 120 min. The experimental setup
315 for the photocatalytic activity test was as follows. The sample (0.5 g), previously cut into pieces

316 (approx. 1×1 cm^2), was immersed in an aqueous dye solution (50 mL, 10 mg/L, pH$_{RB}$ = 5.00,
317 pH$_{AO7}$ = 5.25, pH$_{MR}$ = 1.40). Before illumination, such an assembled system was stirred (3 rpm)
318 in the dark for 15 min to establish adsorption-desorption equilibrium (*zero point*). The
319 photocatalytic performances of the nanocomposites were examined by following the
320 decolourization efficiency of the test dye molecules, where aliquots were taken at the exact
321 illumination time: zero point (0 h) and after 60, 120, 180, 240 and 300 min for RB and AO7 as
322 well as after 20, 40, 60, 80, 100 and 120 min for MR. The sampling volume was 1 mL. The distance
323 between the lamp (ULTRA-VITALUX lamp, 300 W, *Osram, described in detail in section 2.2.2.*)
324 and the samples was set to 30 cm, while the optical power measurements (*R-752 Universal*
325 *Radiometer Readout*, sensor model: *PH-30 DIGIRAD*) showed a value of 30 mW/cm^2. Photolysis
326 of all three dyes was insignificant (less than 1% during the total illumination time) and the same
327 trend was maintained in the system with the CO control sample. The schematic representation of
328 the photocatalytic setup is given in the *Supplementary Information (Fig. 1)*.
329 The percent of photocatalytic degradation (PD) was estimated according to the following
330 expression:

331
$$PD(\%) = \frac{C_0 - C}{C_0} \cdot 100$$

332 where C$_0$ is the initial concentration of the dye solution (*zero point*) and C is the concentration of
333 the dye solution in the selected illumination time interval.

334 In the course of the photocatalytic performances, *the reusability* was also examined. Namely,
335 the reuse test was carried out in three cycles as follows. After performing the primary
336 photocatalytic activity test (described above), the samples were dried at room temperature.
337 Subsequently, each reuse cycle was performed in the same manner as the primary test (before
338 recycling), only with the sampling difference: aliquots were taken at the zero point (0h) and at the
339 end of each cycle (300 min for RB and AO7 and 120 min for MR). Between cycles, the samples
340 were dried at room temperature. The chemical structures of RB, AO7, and MR are given in *Figs.*
341 *6 - 8*.
342
343   *3. Results & Discussion*
344
345 *Colloidal TiO$_2$ and TiO$_2$/Ag NPs*
346
347 With an aim to successfully deposit Ag NPs on the surface of cotton fibers, formerly modified
348 with TiO$_2$ NPs, we have predefined the conditions in the process of reduction of Ag$^+$ ions on the
349 surface of colloidal TiO$_2$ NPs. Before deposition the NPs to the cotton fabric and forming the
350 nanocomposites, both TiO$_2$ and TiO$_2$/Ag NPs were synthesized and characterized.
351
352

3.1. Morphological properties

The shape, size and size distribution of colloidal TiO_2 NPs (before Ag photodeposition) and composite TiO_2/Ag NPs were fully defined using TEM. Representative TEM micrographs of these NPs and corresponding particle size distributions are presented (*Fig. 1*).

The faceted TiO_2 NPs with a narrow particle size distribution and with most dimensions of 4.5 nm were obtained (*Fig. 1c*). The uniformity and narrow size distribution of the aggregated TiO_2/Ag NPs, mostly 8 nm in size, was also proven (*Fig. 1d*).
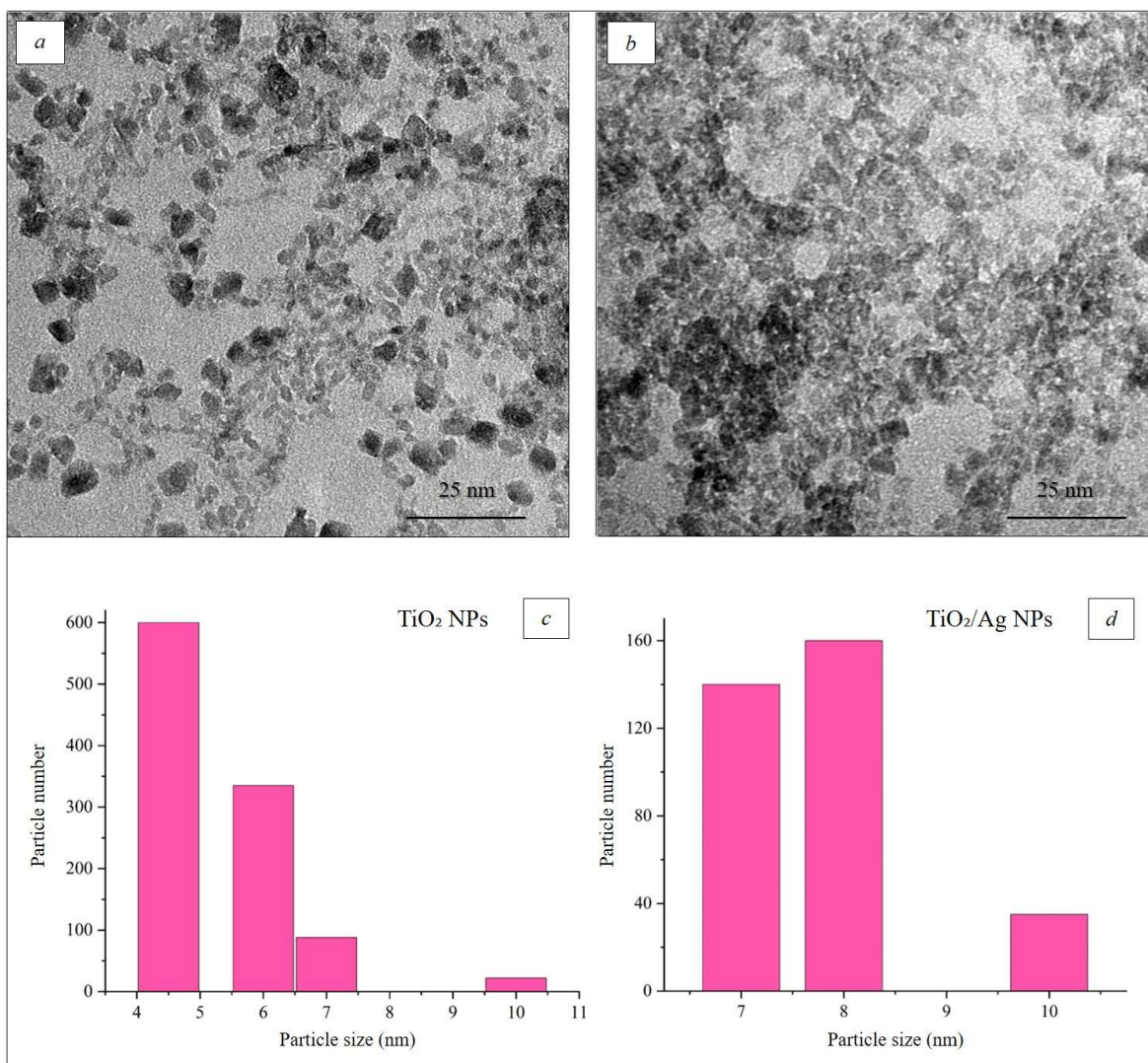
Fig. 1. *The TEM micrographs of colloidal TiO_2 (a) and TiO_2/Ag NPs (b)*
and the appropriate particle size distributions (c and d).

3.2. Optical properties

370

371   The colloidal TiO$_2$ NPs, surface modified with the amino-acid alanine, were illuminated in

372   the presence of Ag$^+$ ions and methanol as a hole scavenger. The absorption spectra of these NPs,

373   along with the TiO$_2$/Ag NPs colloidal dispersion obtained for different illumination times, are

374   presented (*Fig. 2*).

375
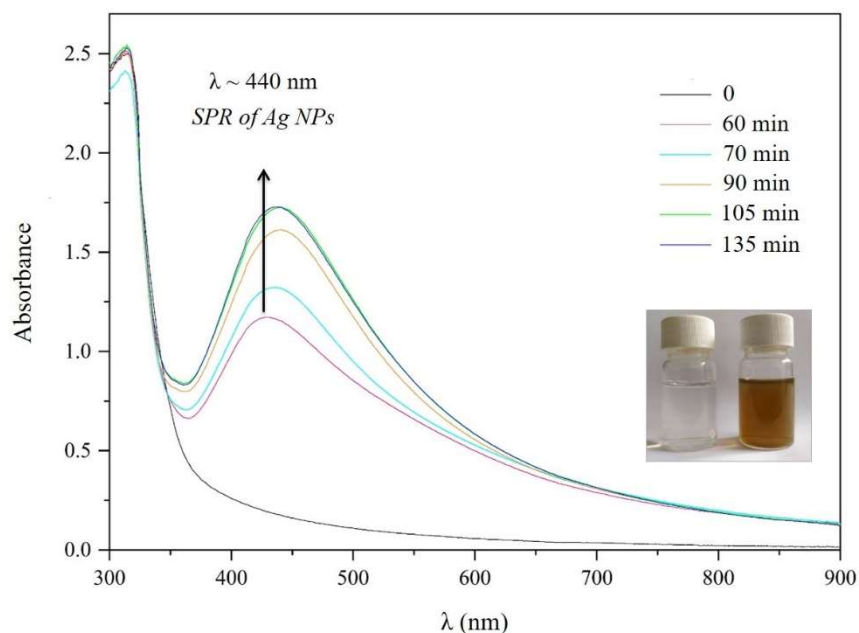
376

377   **Fig. 2.** *The UV/Vis spectra of TiO$_2$/Ag NPs colloidal dispersion for different illumination times.*

378

379   Before illumination, only the absorption corresponding to the colloidal TiO$_2$ NPs surface

380   modified with alanine was observed. However, after 60 min of illumination of TiO$_2$/Ag NPs

381   colloidal dispersion, the characteristic surface plasmon resonance (SPR) of Ag NPs appeared at ~

382   440 nm. Further illumination of the colloidal dispersion led to a significant increase in the intensity

383   of the plasmon peak due to the additional reduction of Ag$^+$ ions, reaching its maximum value after

384   105 min for the applied concentration. Additional illumination didn't increase the intensity of the

385   SPR peak, which would indicate a complete reduction of the present Ag$^+$ ions. The inset in *Fig. 2*

386   clearly shows the yellow/brownish colour of the transparent and stable colloidal dispersion of

387   TiO$_2$/Ag NPs, attributed to the SPR of Ag NPs only of a few nanometres in size (Rivero *et al.*

388   2015). Likewise, in *Fig. 2*, the half-width at half-height of the Ag SPR band increases with

389   increasing illumination time (*redshift*). Namely, the resulting changes in optical properties were

390   caused by an increase in the size of TiO$_2$/Ag NPs due to the amount of reduced Ag$^+$ ions on the

391   surface of TiO$_2$ NPs and, consequently, their agglomeration level.

392   Chemical interaction between individual components, as well as potential binding structure

393   of Ag to the surface of alanine modified colloidal TiO$_2$ NPs (Fig. 4, Fig. 5 in Supplementary

394   Information) is part of our previous investigation published in a reference Milošević et al., 2014.

395 *Nanocomposites*

396   The characterization of the obtained $CO+TiO_2$, $CO+TiO_2/Ag$ and $CO+TiO_2/Ag/TiO_2$
397 nanocomposites and a systematic examination of the photocatalytic activity testing is given below.
398
399   *3.3. Morphological properties, EDX and ICP – OES analysis*
400
401   The surface morphology of cotton fibers coated with TiO_2/Ag and $TiO_2/Ag/TiO_2$ NPs was
402 analysed by FESEM (*Fig. 3*). Comparing the FESEM images of the smooth surface of cotton fibers
403 and the NPs-modified fibers, it is obvious that NPs deposition significantly impacts the surface
404 morphology of cotton fibers. Namely, a strong effect is manifested by the formation of uniform
405 TiO_2/Ag and $TiO_2/Ag/TiO_2$ nano-coatings on the surface of the cotton fiber with a narrow particle
406 size distribution, whose average dimensions of approximately 10 nm are in good agreement with
407 TEM analysis.
408
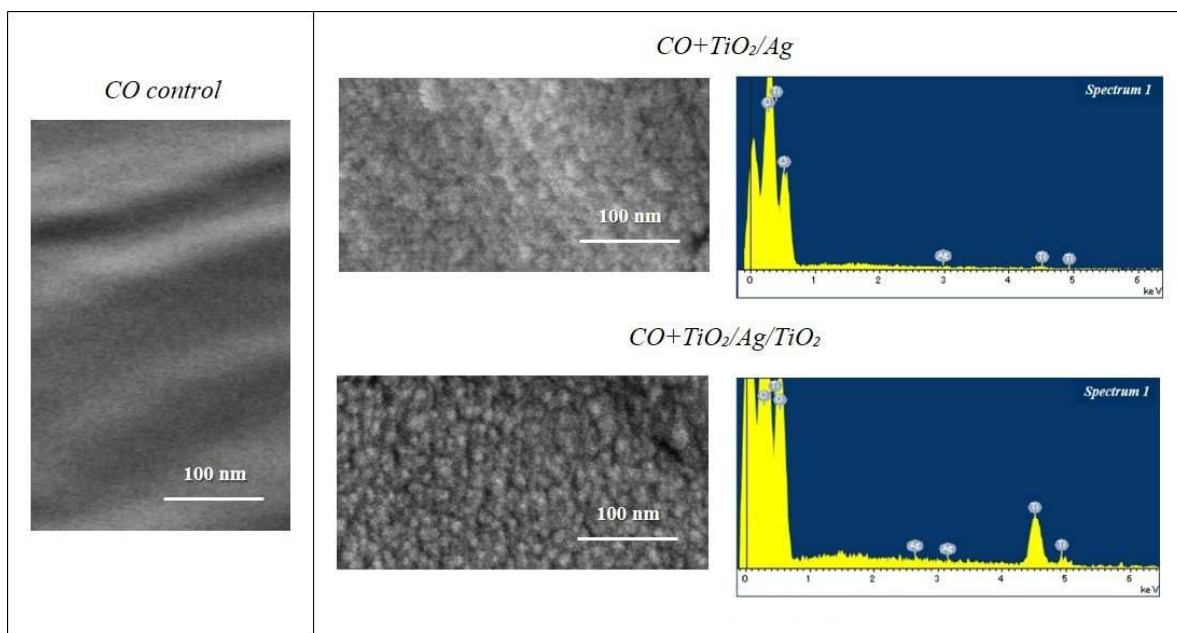
410 **Fig. 3.** *The FESEM micrographs of cotton fiber (CO control) and cotton fibers coated with TiO_2/Ag*
411 *and $TiO_2/Ag/TiO_2$ NPs along with their respective EDX spectra.*
412

413   The surface elemental analysis (submitted in *Fig. 3*, *Table 1*) revealed that the subsequent
414 deposition of TiO_2 NPs on the $CO+TiO_2/Ag$ sample reflected in the increased Ti concentration in
415 the order of magnitude. On the other hand, a manifested decrease in Ag concentration in the
416 $CO+TiO_2/Ag/TiO_2$ (double-layer) sample was expected, considering that the EDX mode of
417 FESEM is a surface-responsive technique.
418
419

420   ***Table 1.*** *The surface elemental composition of nanocomposites based on EDX analysis.*

Element	CO+TiO$_2$/Ag	CO+TiO$_2$/Ag/TiO$_2$
	Atomic concentration [%]	
Ti	0.47	4.90
Ag	0.06	0.01

421

422   The total content of deposited Ti and Ag on the examined samples was determined by ICP -
423 - OES measurements. The obtained results showed almost the same quantity of Ti in samples with
424 TiO$_2$ single-layer deposition: CO+TiO$_2$ (5595.0 $\pm$ 45.0 µg/g) and CO+TiO$_2$/Ag (5549.0 $\pm$
425 $\pm$ 62.0 µg/g), thus proving the reproducibility of the applied synthetic approach and the stability
426 of the TiO$_2$ NPs coatings on the surface of cotton fibers before and after Ag deposition during the
427 photoreduction process. The subsequent deposition of TiO$_2$ NPs, the CO+TiO$_2$/Ag/TiO$_2$ sample,
428 was confirmed by the doubled amount of Ti in the mentioned sample (11191.0 $\pm$ 93.0 µg/g),
429 compared to the CO+TiO$_2$/Ag sample (5549.0 µg/g). The presence of Ag was proven in both
430 samples: CO+TiO$_2$/Ag (217.0 $\pm$ 31.0 µg/g) and CO+TiO$_2$/Ag/TiO$_2$ (170.5 $\pm$ 15.5 µg/g). A slight
431 difference in the measured amount of Ag fits well with the calculated standard deviations.

432

433   *3.4. Structural analysis*

434

435   The structural fingerprint of TiO$_2$ in the synthesized nanocomposites was obtained by Raman
436 spectroscopy. The Raman spectra of CO+TiO$_2$, CO+TiO$_2$/Ag and CO+TiO$_2$/Ag/TiO$_2$ samples
437 with assigned vibrations are presented in *Fig. 4*. The Raman spectra of the CO+TiO$_2$ sample is
438 dominated by peaks characteristic for cellulose macromolecules that comprise cotton material.
439 Namely, typical bands of neat cellulose are defined as follows. The most intensed bands, observed
440 at 2897 and 1096 cm^{-1}, indicate CH and CH$_2$ stretching in cellulose macromolecules (Eronen *et*
441 *al.* 2009; Cabrales *et al.* 2014) as well as C-O-C (symmetric and asymmetric) stretching mode of
442 β (1 - 4) glycosidic bonds between the glucopyranose rings of cellulose (Wiley and Atalla 1987;
443 Abid *et al.* 2017), respectively. These bands are followed by less intensive bands at 1380 cm^{-1}
444 related to CH$_2$ asymmetric stretching of cellulose (Liu *et al.* 1998; Cabrales *et al.* 2014) and bands
445 at 1121 and 520 cm^{-1} attributed to C-O-C glycosidic bond symmetric stretching (Cabrales *et al.*
446 2014). In addition, all other bands characteristic for the Raman vibration of cellulose
447 macromolecules are observed in the spectra of CO+TiO$_2$ sample (Liu *et al.* 1998; Schenzel *et al.*
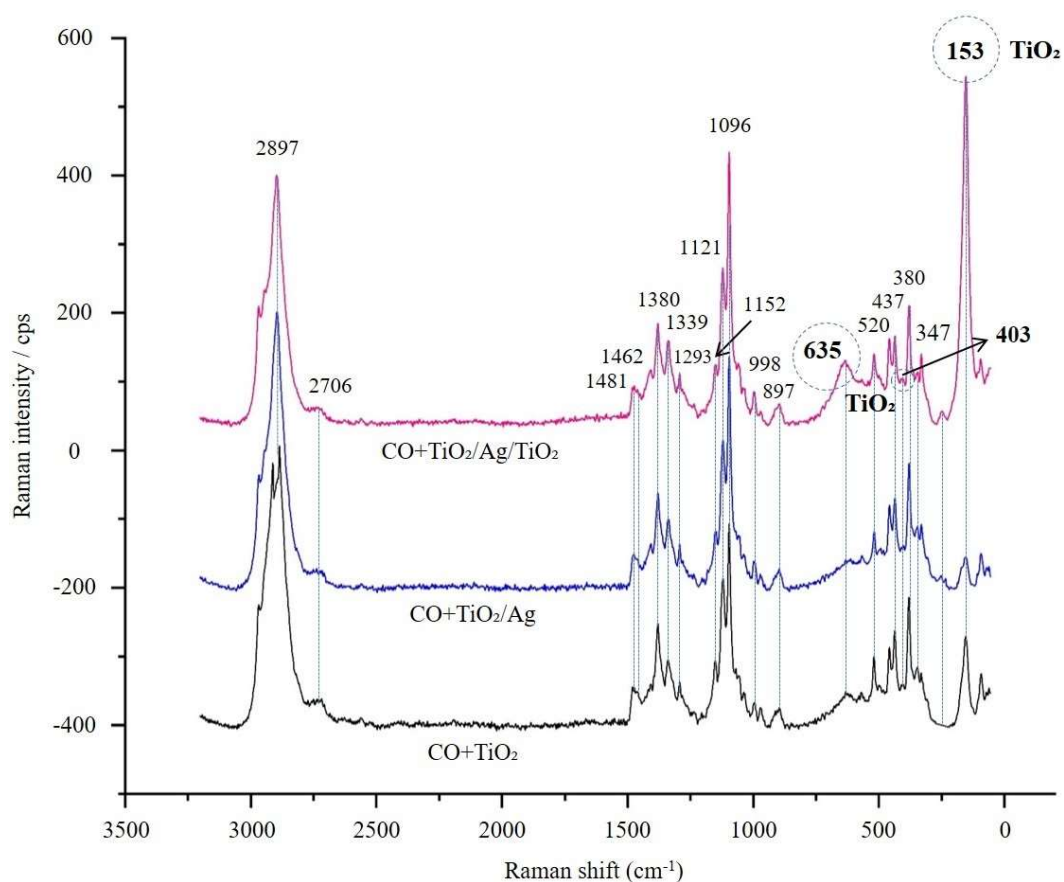448 2005; Agarwal *et al.* 2009; Cabrales *et al.* 2014).

449

450

451

452

453 The strong peak appearing at 153 cm^{-1} as well as weaker peaks at 403 and 635 cm^{-1} following
454 it are assigned to TiO$_2$ anatase Raman active modes, confirming the successful deposition of TiO$_2$
455 on cotton fibers. The band at 153 cm^{-1} is designated to the stretching vibration of the O-Ti-O bond
456 (vibrational E$_g$ phonon, low-frequency) (Ohsaka *et al.* 1978; Abid *et al.* 2017). It should be noticed
457 that these peaks are shifted relative to E$_g$ and B$_{1g}$ vibrations of anatase TiO$_2$ at 144, 399 and 639
458 cm^{-1}, as reported in the literature (Ohsaka 1980; Choi *et al.* 2005). Other characteristic Raman
459 active modes of anatase TiO$_2$ at 513 (A$_{1g}$) and 519 (B$_{1g}$) cm^{-1} (Ohsaka 1980; Choi *et al.* 2005)
460 were not observed in the spectra of the CO+TiO$_2$ sample due to overlap with the C-O-C symmetric
461 stretching of the glycosidic bond in cellulose macromolecules (Cabrales *et al.* 2014). Comparing
462 the Raman spectra of the CO+TiO$_2$/Ag and CO+TiO$_2$/Ag/TiO$_2$ samples, a significant increase in
463 the intensity of the bands at 153 and 635 cm^{-1} is observed. This observation is fully in line with
464 single- and double-loading of TiO$_2$ NPs in these cotton samples.

465 Crystalline structure of samples (CO and CO+TiO$_2$/Ag/TiO$_2$) was studied by XRD analysis.
466 The peaks characteristic for the cellulose crystal structure are observed (Keshk et al. 2019).
467 Obtained results showed the presence of anatase crystalline structure of TiO$_2$ NPs with low domain
468 of crystallinity (Radoičić et al. 2017) and face centred cubic structure of Ag NPs (Meng 2015).
469 XRD pattern is shown in Fig. 2 in the Supplementary Information.

470

3.5. Optical properties

472

473   The successful deposition of Ag NPs on the cotton fabric surface modified with TiO$_2$ NPs
474   was tested by measuring diffuse reflectance electronic spectra and the corresponding spectra for
475   CO control, CO+TiO$_2$/Ag and CO+TiO$_2$/Ag/TiO$_2$ samples are presented (*Fig. 5*).

476   The addition of Ag caused significant changes in the absorption spectra of the CO+TiO$_2$
477   sample in the visible range. The appearance of a band (shoulder) at $\lambda \sim 440$ nm in the reflectance
478   spectra of the CO+TiO$_2$/Ag and CO+TiO$_2$/Ag/TiO$_2$ samples is characteristic of the SPR absorption
479   of Ag NPs only of a few nanometres in size (Rivero *et al.* 2015). The band width is a direct
480   consequence of Ag NPs agglomeration on the fiber surface. The lower band intensity in the
481   CO+TiO$_2$/Ag/TiO$_2$ sample compared to the CO+TiO$_2$/Ag sample is an outcome of the subsequent
482   application of TiO$_2$ NPs. After deposition of Ag NPs, the cotton sample appears brownish, while
483   macroscopic observation of the sample after sequent application of TiO$_2$ NPs indicates a fainter
484   hue. The obtained result strongly confirms the successful fabrication of Ag NPs and additional
485   amounts of TiO$_2$ NPs on CO+TiO$_2$/Ag/TiO$_2$ samples.

486

487

488
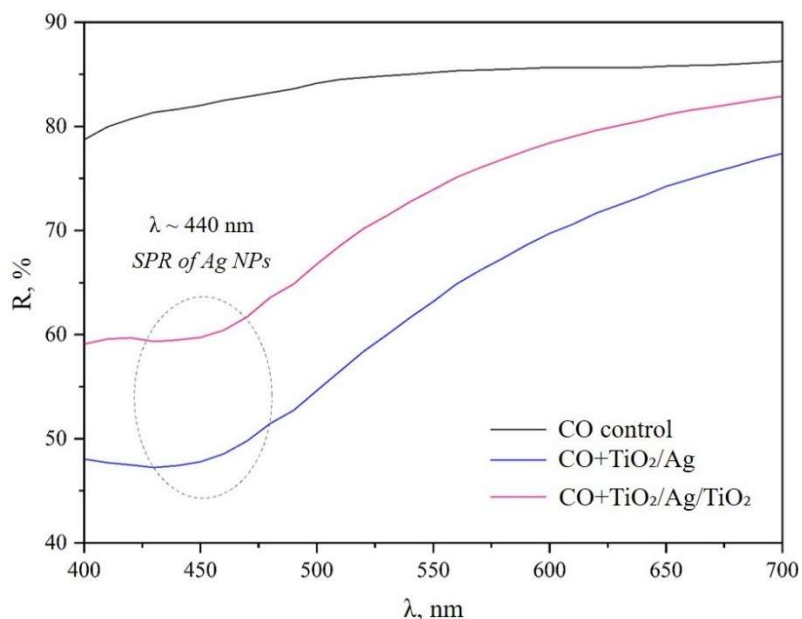
489   **Fig. 5.** *The DRS of the CO control, CO+TiO$_2$/Ag and CO+TiO$_2$/Ag/TiO$_2$ samples.*

490

491   *3.6. Photocatalytic activity test*

492

493   The photocatalytic efficiency of nanocomposite textile materials has been tested following
494   the decomposition process of three organic dyes: RB, AO7 and MR, as dyes utilized in the textile
495   industry.

496

497   *Rhodamine B*

498

499   The concentration changes of RB solution during illumination in the dye/fabric system were
500   determined by measuring the absorption intensity (λ_{max}) of RB at 554 nm (*Fig. 6*). The obtained
501   results manifest that ~ 30% of RB decolourization was achieved after 60 min of illumination in
502   the presence of CO+TiO$_2$ and CO+TiO$_2$/Ag samples and even 50% in the presence of
503   CO+TiO$_2$/Ag/TiO$_2$ sample, when the transition of RB to Rhodamine form occurs (Watanabe *et al.*
504   1977) (*Table 2*). Matter-of-fact, two pathways are characteristic for the RB photodegradation: 1)
505   cleavage and destruction of the conjugated chromophore structure, followed by a decrease in
506   absorbance while the position of the main peak remains the same and 2) a hypsochromic shift of
507   the absorbance maximum, as a result of N-deethylation process (Ma and Yao 1998; Park and Choi
508   2005; Wang *et al.* 2008; Yu *et al.* 2009; Fan *et al.* 2012). The second scenario goes through the
509   gradual transition of RB (N,N,N',N'-Tetraethyl-rhodamine, 554 nm) to N,N,N'-Triethyl-rhodamine
510   (539 nm), N,N'-Diethyl-rhodamine (522 nm), N-Ethyl-rhodamine (510 nm) finally reaching
511   Rhodamine (498 nm) as the major intermediate (Watanabe *et al.* 1977; Fan *et al.* 2012).
512   Rhodamine B to Rhodamine blue-shift transition was observed in the case of all three
513   nanocomposites and the suitable absorption intensities are given as an example for the
514   CO+TiO$_2$/Ag sample (*Fig. 6b*). Furthermore, the maximum photocatalytic activity (over 90%) in
515   the degradation process of RB was achieved with the CO+TiO$_2$/Ag/TiO$_2$ sample at a final
516   illumination time of 300 min, when decolourization of all Rhodamine forms occurs. The obtained
517   photocatalytic efficiency of the TiO$_2$ double-loaded sample was even 30% more compared to the
518   single-loaded samples. Thus, regardless of the complex and anthraquinone-like structure of RB,
519   which as a rule complicates photodegradation (Khataee and Kasiri 2010), the presence of certain
520   functional groups in the RB structure enables good contact between the dye and the TiO$_2$ catalyst.
521   Namely, TiO$_2$ NPs are known to have a high affinity towards –COOH groups and O atoms in the
522   RB crystal lattice (Goddard *et al.* 2012). Besides, the presence of Ag NPs (scavenger of
523   photogenerated e$^-$ which hinder e$^-$/h$^+$ recombination) on their surface significantly contributes to
524   the increase of photocatalytic activity. An additional improvement of the photocatalytic properties
525   descends from the good adsorption of Ag on the nitrogen atom of the RB molecule as well as from
526   the weak steric hinderence that allows adequate access of Ag.
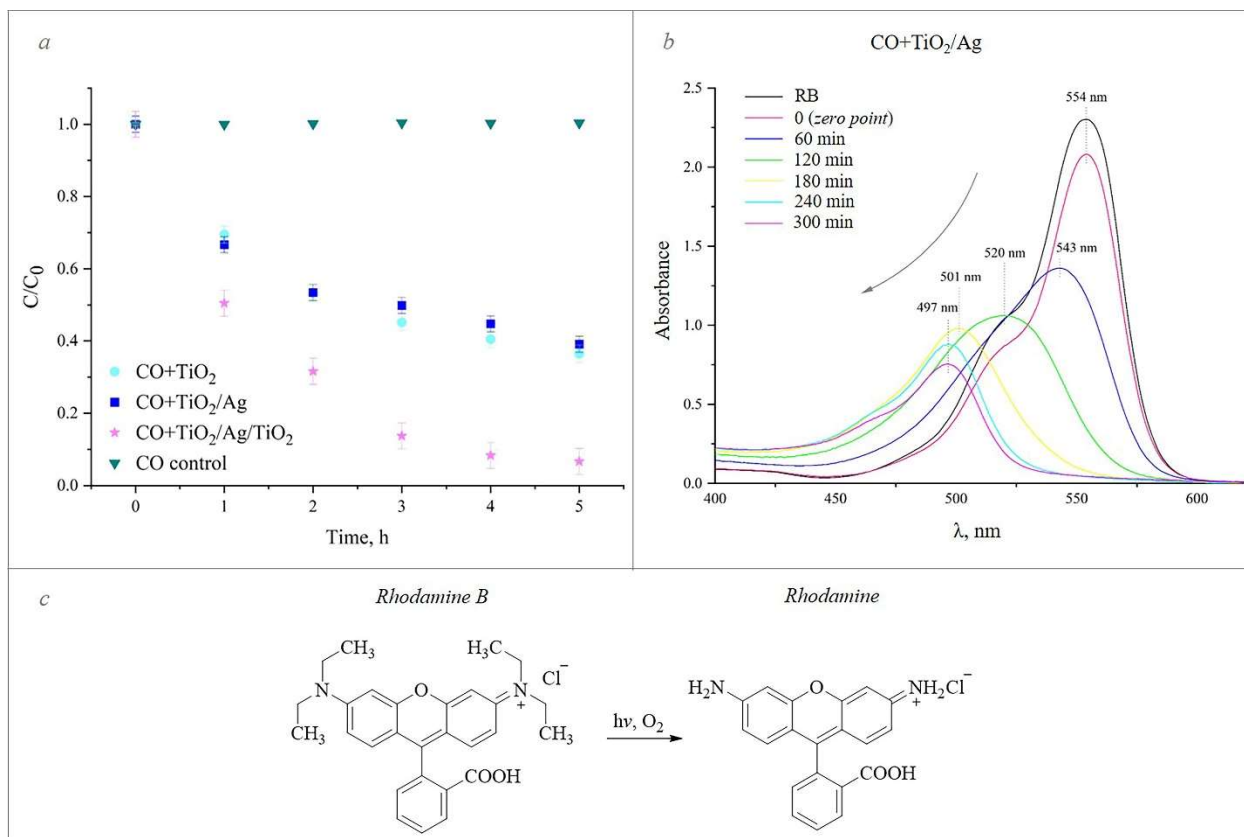
Fig. 6. *The photodegradation curves (C/C₀) of Rhodamine B for the tested samples (a), absorption spectra of Rhodamine B (554 nm) to Rhodamine (497 nm) blue-shift transition for CO+TiO₂/Ag sample (b), N-deethylation process of Rhodamine B to Rhodamine (Schmid 2004) (c) and suitable wavelenghts changes during the photocatalysis of Rhodamine B (d).*
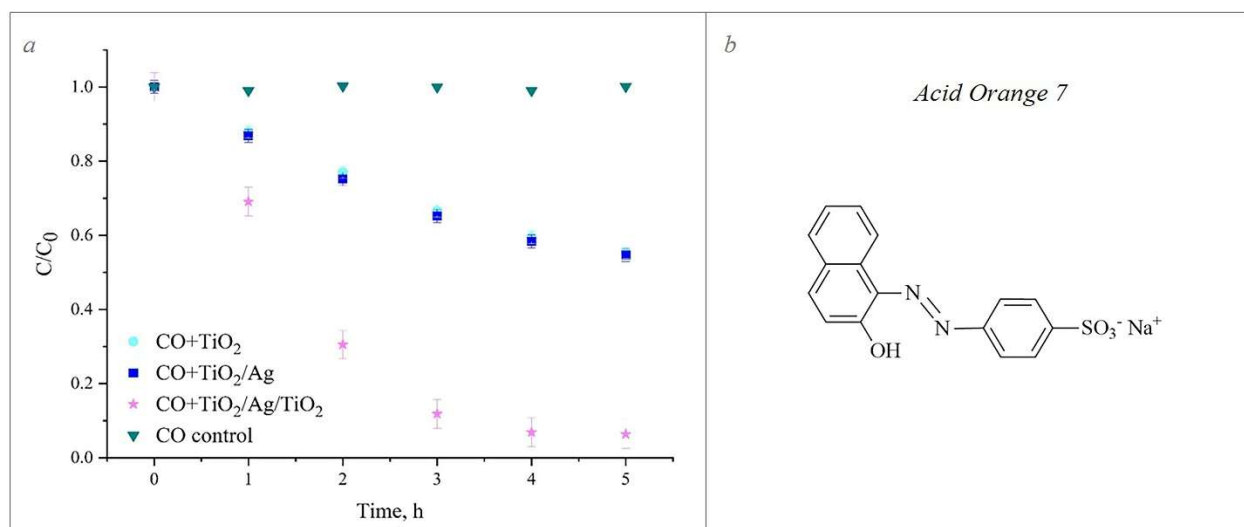
Acid Orange 7

The concentration changes of the AO7 solution in the presence of the tested samples during illumination were accompanied by a variation in the intensity of the absorption spectra of AO7 at $\lambda_{max} = 485$ nm (*Fig. 7*). The photocatalytic efficiency was drastically lower than in the case of RB, as only 7 - 9% AO7 decolourization was achieved after 60 min of illumination for the CO+TiO₂ and CO+TiO₂/Ag samples, and $\sim$ 30% for the CO+TiO₂/Ag/TiO₂ sample (*Table 2*). However, after 300 min of illumination, the photocatalytic efficiency of the CO+TiO₂/Ag/TiO₂ sample reached over 90%, which is even 50 - 60% higher than for the other samples. The worse degradation properties of AO7 compared to RB, with the exception of CO+TiO₂/Ag/TiO₂ sample, can be attributed to the differences in the chemical structure of these organic dyes (*Figs. 6 - 8*). The literature explanation for the good dye sorption and upcoming degradation of AO7 was expected due to three main factors. First of all, acidic conditions favour the electrostatic interaction between the positively charged TiO₂ NPs and the negatively charged sulfonate group of the dye molecule (Marković *et al.* 2015) *via* the formation of a bidentate inner sphere surface complex (Bauer *et al.*

549 1999; Bourikas *et al.* 2005). However, there is an opposite view to this claim, where the presence
550 of the -SO$_3^-$ group in AO7 is probably the origin of reduced dye-sorption to fabrics, which may
551 consequently lead to a decrease in photocatalysis efficiency (Khataee and Kasiri 2010). A review
552 published by *Khataeea and Kasiri* highlights the difficulties in examining the influence of the
553 sulfonic group, due to the competitive processes described in the aforementioned study (Khatae
554 and Kasiri 2010). Second, the presence of the -OH group in the AO7 structure and its accessibility
555 to TiO$_2$ NPs favours dye degradation. In particular, the presence of -N=N- group, as a potential
556 binding site for Ag, is also a reason for good dye sorption. Particularly, -N=N- and C-
557 N= bonds are susceptible to photodegradation because they act as a target area near the dye
558 chromophore in the TiO$_2$/Ag-mediated photodegradation system (Khataee and Kasiri 2010).
559 However, the major steric hindrance of the -N=N- group in AO7 molecules (surrounded by two
560 benzene rings) obstructs access of Ag to the nitrogen atom, in contrast to the RB molecules where
561 the nitrogen atom is surrounded by -CH$_2$CH$_3$ groups (besides one benzene ring).

562   A multitude of parameters can affect the photodegradation of dyes using TiO$_2$ NPs (pH, dye
563 type, initial dye concentration, types of dye functional groups, photocatalyst concentration,
564 photocatalyst particle size, light intensity, temperature, the presence of electron acceptors) (Reza
565 *et al.* 2017). Hence, a crucial step for efficient photocatalysis may be the adsorption of target
566 molecules on the surface of immobilized TiO$_2$ or TiO$_2$/Ag NPs and the corresponding interactions
567 between the functionality of those molecules and the photocatalyst surface science.
568
569

571 ***Fig. 7.*** *The photodegradation curves (C/C$_0$) of Acid Orange 7 for the tested samples (a),*
572 *chemical structure of Acid Orange 7 (b).*
573
574
575
576

577   *Methyl Red*

578

579   The concentration changes of the MR dye solution in the presence of the tested samples
580   during illumination were followed by intensity changes in the MR absorption spectra at $\lambda_{max} = 520$
581   nm (*Fig. 8*). Considering the obtained results, it can be noticed that a significantly shorter
582   illumination time is required for the decolourization of the MR dye. Namely, about 35% MR
583   decolourization was achieved after only 30 min of illumination for the CO+TiO$_2$ and CO+TiO$_2$/Ag
584   samples and about 10% more for the CO+TiO$_2$/Ag/TiO$_2$ sample (*Table 2*). The most efficient
585   photocatalyst was the CO+TiO$_2$/Ag/TiO$_2$ sample in the presence of which 90% of the MR dye was
586   degraded in two hours. Namely, MR molecules possess a –COOH functional group as a binding
587   site for TiO$_2$ NPs as well as a –N=N– group either a lone electron pair on the N atom suitable for
588   Ag (*Fig. 8*). Additionally, highly acidic environment (pH$_{MR}$ = 1.40) greatly contributes to the
589   exceptional affinity of TiO$_2$ towards carboxyl group of the MR dye. The present carboxylic moiety
590   in the MR molecule can easily react with H$^+$ *via* the photo-Kolbe reaction resulting in a more
591   efficient rate of photodegradation of this dye (Khataee and Kasiri 2010). The outstanding
592   enhancing of the photocatalytic properties of the synthesized nanocomposites, in this instance,
593   refers to the better achieved contact between TiO$_2$ and Ag NPs and the MR dye. Namely, the
594   anionic nature of the dye molecules accelerates the interaction with positively charged TiO$_2$ NPs
595   in an acidic medium. As in the case of previously tested dyes, the TiO$_2$ double-loaded cotton fabric
596   played a major role in improving the photocatalytic efficiency of the nanocomposite textile
597   materials. Regardless of the structural dyes differences, it is evident that the mentioned distinctions
598   can be overcome by photocatalysis mediated by TiO$_2$/Ag/TiO$_2$ NPs.

599

600
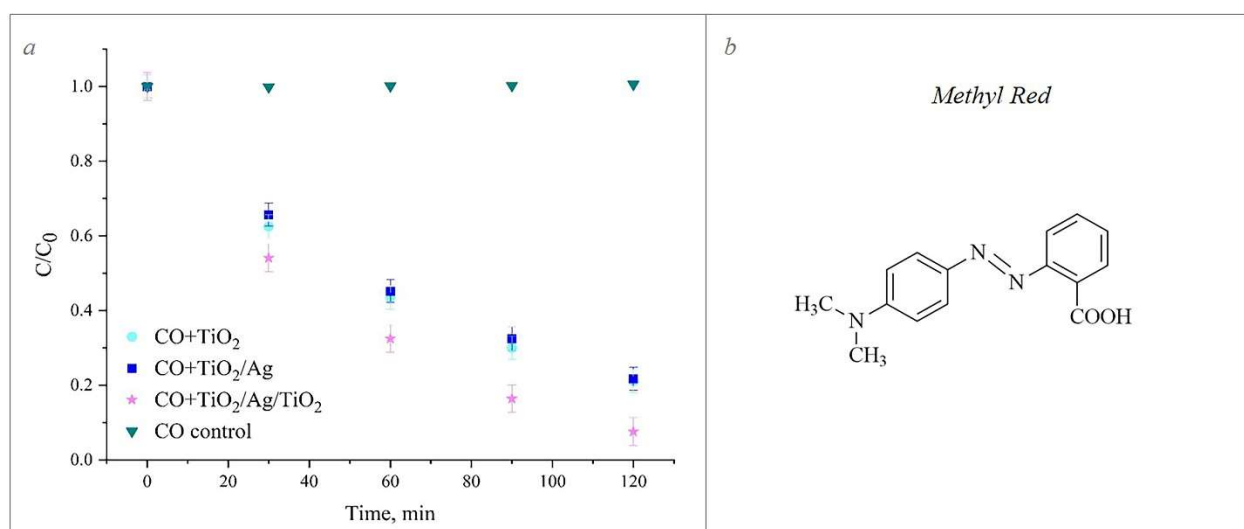
601

602   **Fig. 8.** *The photodegradation curves (C/C$_0$) of Methyl Red for the tested samples (a),*
603   *chemical structure of Methyl Red (b).*

604

605   ***Table 2.*** *The photocatalytic degradation of Rhodamine B, Acid Orange 7 and Methyl Red.*

Photocatalytic degradation of Rhodamine B, PD(%)						
Nanocomposite	*Illumination time* (min)					
	60	120	180	240	300	σ
CO+TiO$_2$	30.5	46.7	54.8	59.5	63.6	23.9
CO+TiO$_2$/Ag	33.3	46.6	50.1	55.3	60.9	22.2
CO+TiO$_2$/Ag/TiO$_2$	49.7	68.4	86.3	91.7	93.3	35.9
Photocatalytic degradation of Acid Orange 7, PD(%)						
Nanocomposite	*Illumination time* (min)					
	60	120	180	240	300	σ
CO+TiO$_2$	6.7	13.4	19.9	24.3	30.5	11.3
CO+TiO$_2$/Ag	9.1	15.4	23.8	33.5	39.5	14.7
CO+TiO$_2$/Ag/TiO$_2$	30.9	69.5	88.2	93.1	93.6	38.8
Photocatalytic degradation of Methyl Red, PD(%)						
Nanocomposite	*Illumination time* (min)					
	30	60	90	120		σ
CO+TiO$_2$	37.5	56.4	70.0	78.9		31.3
CO+TiO$_2$/Ag	34.3	54.8	67.6	78.3		31.0
CO+TiO$_2$/Ag/TiO$_2$	45.9	67.5	83.6	92.4		36.9

606
607

608   From the previous one, in the case of CO+TiO$_2$ sample for all three dyes, photocatalytic
609 degradation under white light is observed (RB - 63.6, AO7 - 30.5, MR –PD(78.9%)). The
610 explanation can be found in the presence of near UV light (4 - 5%) in the solar spectrum, enough
611 for TiO$_2$ NPs to show a certain photocatalytic activity.

612
613
614
615
616

Photoinduced charge separation in TiO₂/Ag/TiO₂-mediated photodegradation system induced by UV and visible light

617 *Photoinduced charge separation in TiO$_2$/Ag/TiO$_2$-mediated photodegradation system induced by*
618 *UV and visible light*
619

620   In the sum of the obtained results, the photocatalytic performances were in the following
621 order in terms of the samples: CO+TiO$_2$/Ag/TiO$_2$ > CO+TiO$_2$/Ag ≥ CO+TiO$_2$. As mentioned, the
622 differences in the photodegradation performances of dyes treated with the same samples occur due
623 to the divergent chemical structures of these molecules, and hence to the individual binding
624 interactions between their functional groups and TiO$_2$/Ag NPs. Further, the CO+TiO$_2$/Ag/TiO$_2$
625 nanocomposite possesses the highest removal efficiency in the case of all tested dyes (> 90%),
626 indicating its exceptional photocatalytic ability. In addition, single-layer processed samples
627 (CO+TiO$_2$, CO+TiO$_2$/Ag) have practically the same removal efficiency of all dyes, emphasizing
628 once more the importance of the stabilizing TiO$_2$ double-layer. Since the photocatalytic
629 decolourization of CO+TiO$_2$/Ag and CO+TiO$_2$ samples is practically imperceptible, and Ag
630 deposition generally increases dye adsorption, it can be assumed that the synthesized Ag NPs act
631 predominantly as e$^-$ traps in the examined CO+TiO$_2$/Ag/TiO$_2$ system.

632   The explanation for the advanced photocatalysis mediated by TiO$_2$/Ag/TiO$_2$ NPs is as follows
633 (outlined schematically in "lower scale" in *Fig. 9*). Namely, semiconductive TiO$_2$ NPs are widely
634 recognized for their extraordinary photocatalytic properties when exposed to adequate irradiation,
635 λ < 390 nm (*Mechanism 1*, *Fig. 9a*). In our previous research (Milošević *et al.* 2013, 2014, 2017)
636 as well as in this study photogenerated e$^-$ from TiO$_2$ NPs are used to synthesize Ag NPs on their
637 surface. Moreover, the immobilized Ag NPs on the surface of TiO$_2$ NPs should enhance the
638 activity of TiO$_2$ photocatalyst as they behave as electron scavengers and hinder e$^-$/h$^+$
639 recombination. This e$^-$ also interact with O$_2$ from the environment to form highly reactive
640 superoxide (O$_2$$^{\bullet-}$) radicals, which further generate hydroxyl (OH$^\bullet$) radicals in the acidic medium
641 and strongly contribute to the oxidation of the dye on the photocatalyst surface. The existence of
642 hot-spots as well as their location at the phase boundary is already known in the literature (Sousa-
643 Castillo *et al.* 2016). In order to further increase the catalytic hot-spots of such a system, one more
644 layer of TiO$_2$ NPs was subsequently applied. Accordingly, the synthesized Ag NPs act as electron
645 traps and scavenge the e$^-$ from the second layer of TiO$_2$. As the trapping of e$^-$ by Ag-metal occurs
646 at a faster rate compared to e$^-$ transfer from TiO$_2$ to O$_2$ or recombination with h$^+$ (Szabó-Bárdos *et*
647 *al.* 2003; Rupa *et al.* 2007), as the main disadvantage of TiO$_2$, enhanced degradation of dyes by
648 reactive oxygen species is indeclinable. Besides the layer structures of TiO$_2$/Ag/TiO$_2$ coating, the
649 total amount of nanocomposites has great effects on the photodegradation capability of dyes.

650   Conversely, upon exposure of the TiO$_2$/Ag/TiO$_2$ nanocomposite to visible light illumination
651 (*Mechanism 2*, *Fig. 9b*), the e$^-$ below the Fermi level (E$_f$) of Ag NPs will be excited to the surface
652 plasmon states (E$_{SPR}$), leaving h$^+$ below the E$_f$ (Leong *et al.* 2014). Thereupon, the contact between
653 Ag and TiO$_2$ NPs ensures e$^-$ transfer from the surface plasmon states of Ag to the CB of TiO$_2$.
654 Generation of collected e$^-$ occurs in the CB of TiO$_2$, since the CB is an electron acceptor.
655 Simultaneously, O$_2$$^{\bullet-}$ anionic radicals are formed, which further build up $^\bullet$HO$_2$ radicals by
656 protonation. The combination of created $^\bullet$HO$_2$ radicals and trapped e$^-$ results in H$_2$O$_2$ and the final

657 formation of photodegradation active oxygenated species such as OH$^{\bullet}$ radicals. Although
658 interference in e^{-} transfer from Ag to TiO$_2$ occurs due to the formation of a Schottky barrier at the
659 metal-semiconductor interface (higher E$_f$ of TiO$_2$ compared to Ag), these e^{-} are proven to be able
660 to transfer due to their strong e^{-} oscillating collectively on the SPR excitation (Leong *et al.* 2014).
661 Interband excitation appears, giving sufficient energy to the e^{-} to overcome the Schottky barrier at
662 the interface (Kochuveedu *et al.* 2013; Xiao *et al.* 2013; Leong *et al.* 2014). Along these lines, e^{-}
663 transfer to the CB of TiO$_2$ is initiated and leads to the enriched formation of OH$^{\bullet}$ radicals, which
664 enhances photocatalytic oxidation (Leong *et al.* 2014). Visible-light-active photocatalysts,
665 designed based on the injection of SPR-induced e^{-} from metal NPs into the CB of TiO$_2$, are also
666 briefly described in reference (Schneider *et al.* 2014). Additionally, the conceptual and detailed
667 mechanisms of photoinduced e^{-} transfer in a semiconductor-metal-semiconductor system
668 involving TiO$_2$/Ag nanocomposites are well designated in citation (Rashid *et al.* 2022). To the best
669 of our knowledge, the lack of literature data in the field of advanced cotton-based TiO$_2$/Ag/TiO$_2$
670 nanocomposites is managed by the promising results obtained in this study.
671

672
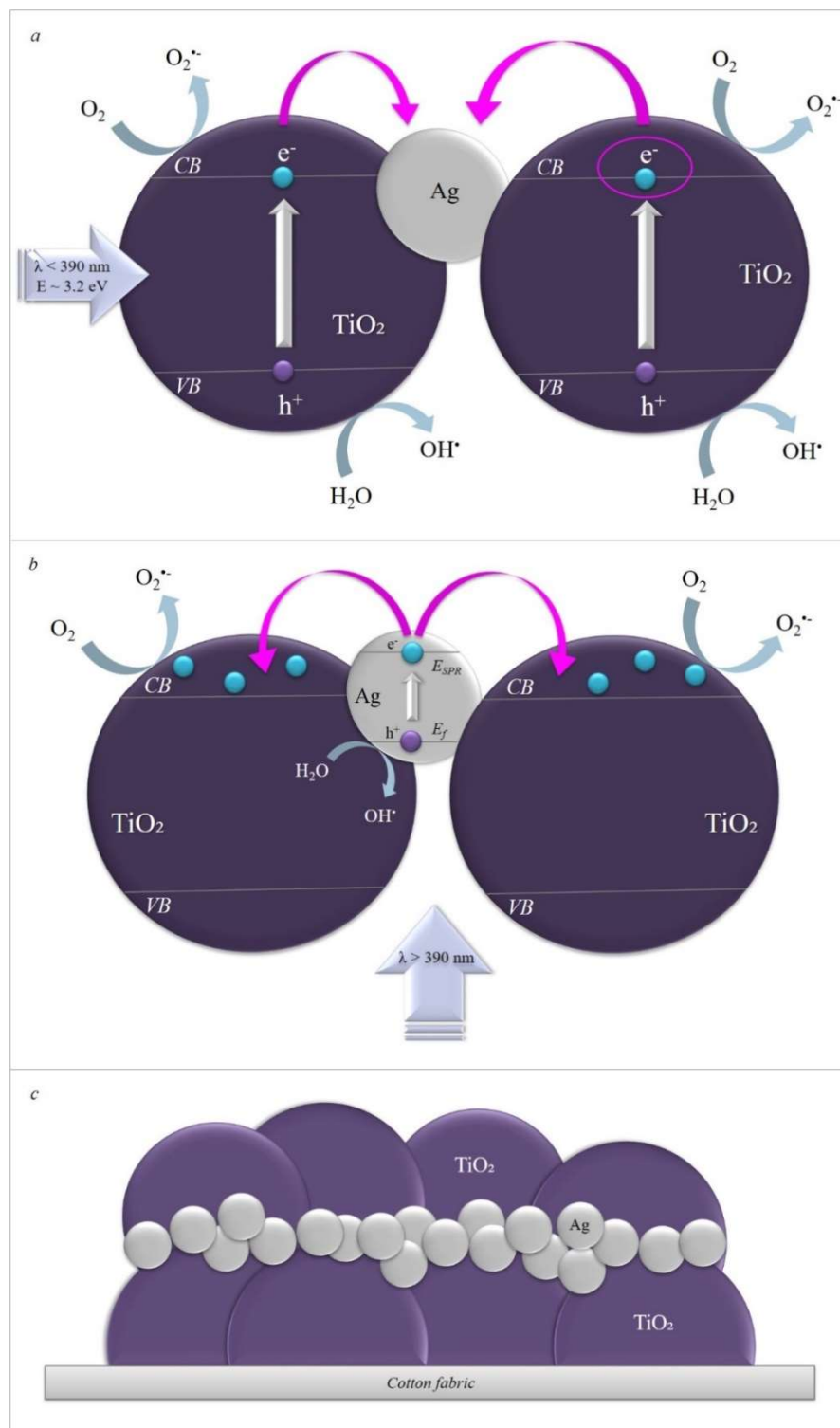
Fig. 9. *The photoinduced charge separation in TiO$_2$/Ag/TiO$_2$-mediated photodegradation system (UV light) - Mechanism 1 (a) photochemical processes on the surface of the synthesized nanocomposite induced by visible light - Mechanism 2 (b) TiO$_2$/Ag/TiO$_2$ NPs modified cotton fabric composite (c).*

676

677   The presented results are consistent with the images of aliquots at specific time intervals for
678 the tested samples and dyes (*Fig. 10*). The displayed images show all aliquots initially tested for
679 24 h (RB and AO7) or 240 min (MR). The final illumination time to achieve the maximum
680 photocatalytic efficiency, which was further preserved, was subsequently adjusted to 300 min (RB
681 and AO7) or 120 min (AO7) (*Figs. 6 - 8*, *Table 2*). These photographs are very informative as they
682 show the colour changes to complete decolourization of the investigated dyes during one
683 photodegradation test cycle. Considering that no discoloration of the dye solution was observed in
684 the case of the control sample (*Fig. 10, row 1*), as expected, the effect of dye decolourization can
685 be attributed to the deposited NPs. According to the literature, colour fading in the samples treated
686 with NPs may be a direct consequence of the photocatalytic destruction of C-N= and/or -N=N-
687 bonds, as these bonds represent sites near the chromophore that are attacked through the
688 photodegradation action (Khataee and Kasiri 2010). The presented result clearly confirms the
689 positive impact of the deposited TiO_2/Ag NPs on the dyes decolourization process, where the
690 colour fading was the most pronounced for the $CO+TiO_2/Ag/TiO_2$ sample and the MR dye,
691 visually proving the benefits of the TiO_2 double-layer deposition over its single processing.
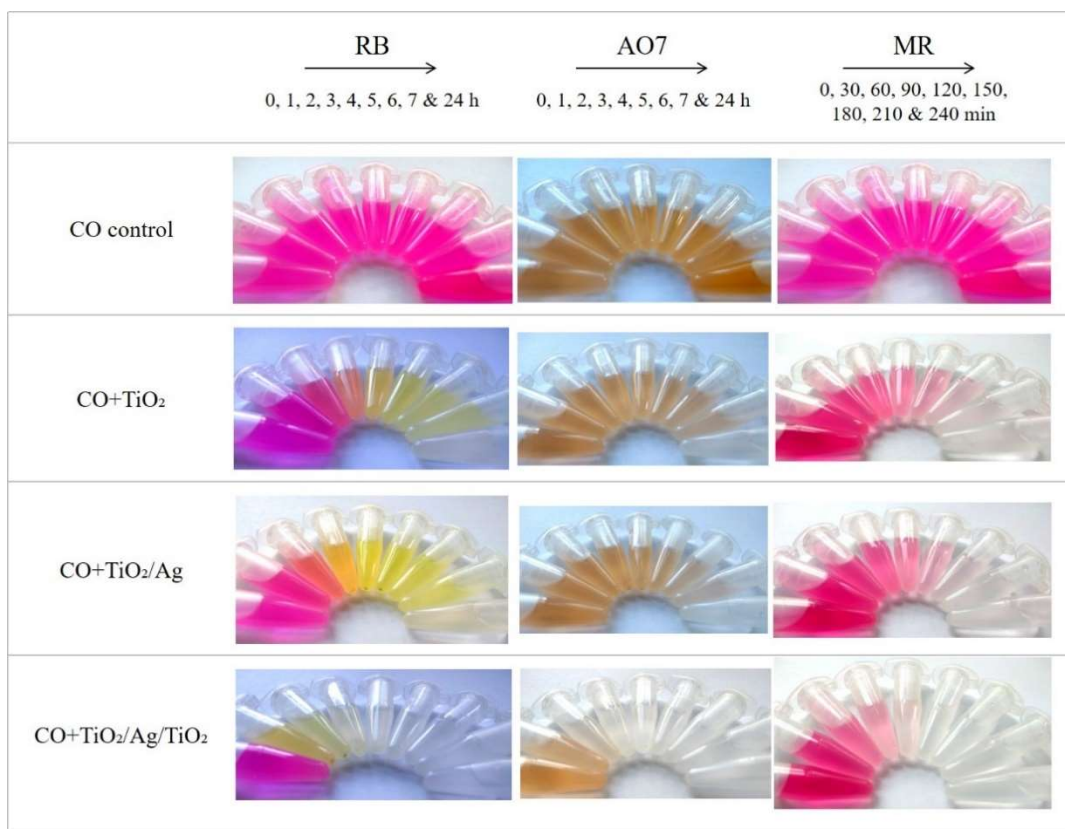
Fig. 10. *The images of aliquots at specific time intervals for the tested samples and dyes.*

696   The images of the tested samples before and after photocatalysis are shown in *Fig. 11*. In the
697 case of control sample, coloring of the samples was observed after the completion of the
698 illumination process, and was a consequence of color adsorption (*Fig. 11, column 1*). However, in

24

699 the samples treated with NPs, only the fading of the original colour is noticeable after the
700 completion of the sorption and photocatalytic processes. Namely, the colour fading of the
701 nanocomposite samples appeared as a consequence of the decolourization of adsorbed dyes.

702 Considering the excellent photocatalytic efficiency of the tested samples, their reuse
703 capability was approached.

704
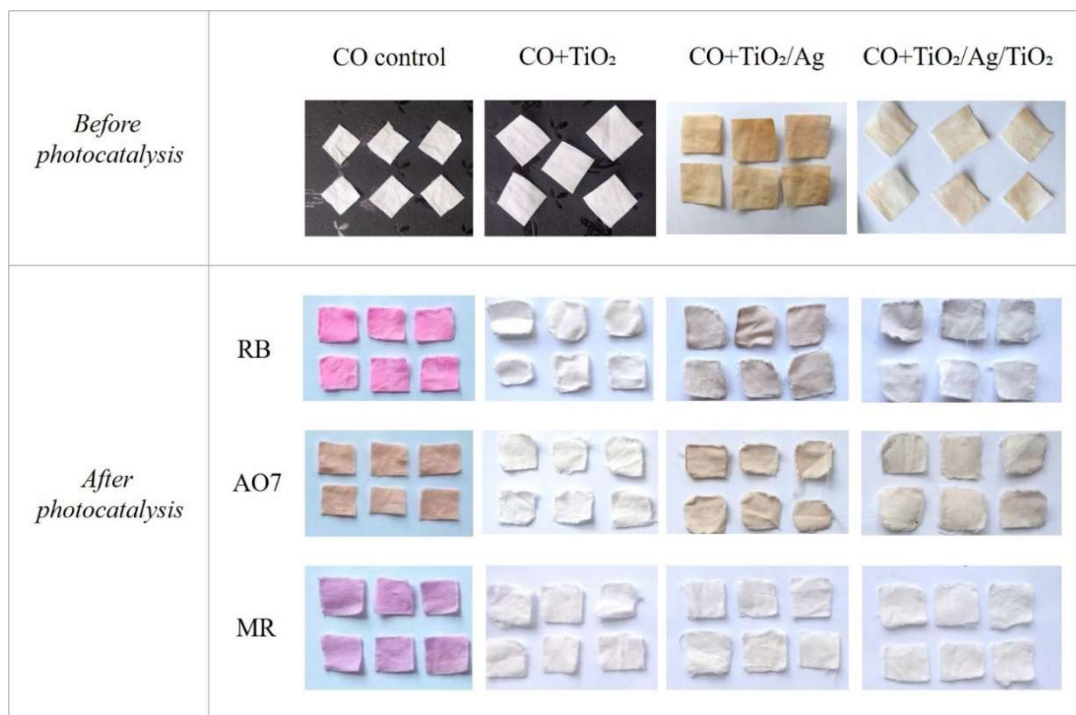
706 **Fig. 11.** *The images of the tested samples before and after photocatalysis.*

707

708 *3.7. Reuse*

709

710 Studying the photocatalytic performances, the highly desirable possibility of multiple use
711 (reuse) of the samples was also tested through three repetitive cycles. The photocatalytic efficiency
712 of the $CO+TiO_2$, $CO+TiO_2/Ag$ and $CO+TiO_2/Ag/TiO_2$ samples after applied reuse cycles is
713 illustrated by the bar charts in *Fig. 12*.

714 As expected, the photocatalytic performances were in the following order regarding the
715 samples: $CO+TiO_2/Ag/TiO_2 > CO+TiO_2/Ag \geq CO+TiO_2$ and in the order of the tested dyes: MR
716 > RB > AO7. Namely, the $CO+TiO_2/Ag/TiO_2$ nanocomposite showed the highest photocatalytic
717 efficiency after the third reuse cycle for all dyes (> 70%), in particular for MR (81.6%), once again
718 indicating its exceptional photochemical ability. However, the photocatalytic performances of the
719 $CO+TiO_2$ and $CO+TiO_2/Ag$ samples were practically the same after each reuse cycle for all dyes,
720 highlighting the importance and efficiency of the mediation with TiO_2 double-layer. A slight
721 decrease in dyes removal efficiency across cycles, when observing the same sample, was expected
722 and consistent with literature data (Radoičić *et al.* 2017).

723

724
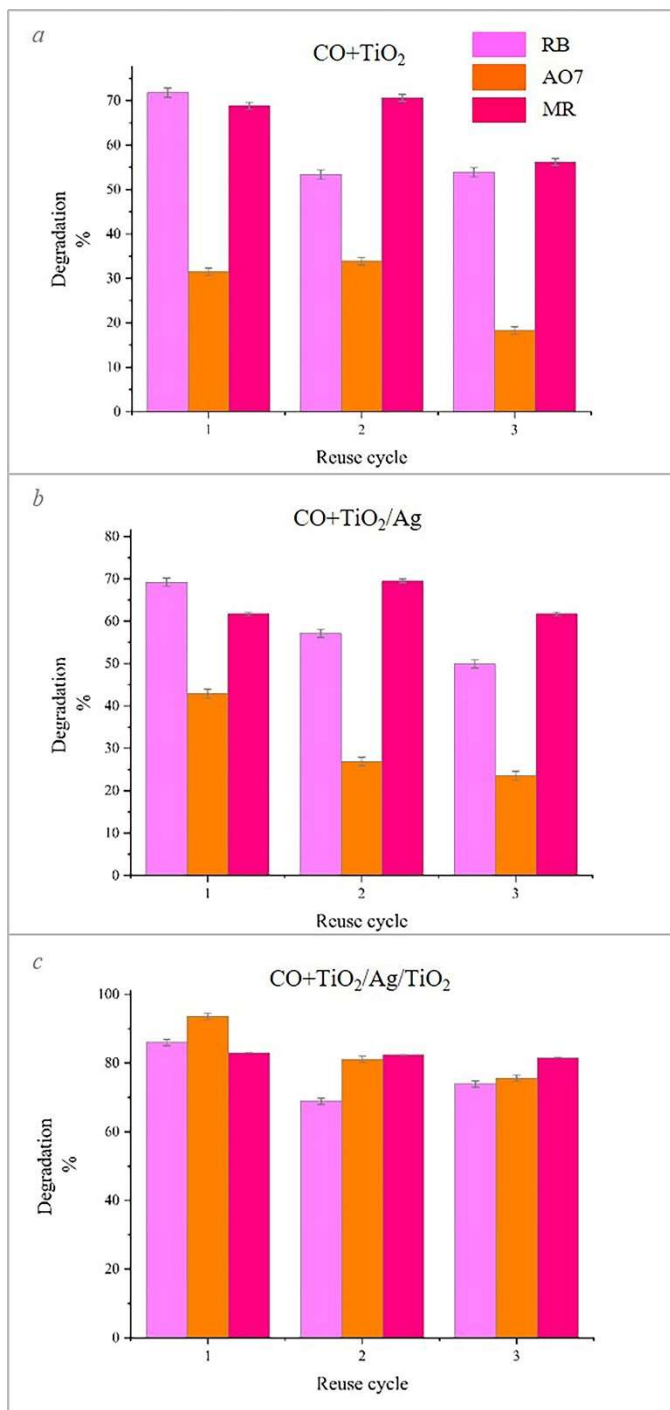
Fig. 12. The photocatalytic efficiency of the $CO+TiO_2$ (a), $CO+TiO_2/Ag$ (b) and $CO+TiO_2/Ag/TiO_2$ (c) samples after three reuse cycles (illumination time: 300 min for RB and AO7, 120 min for MR).

725
726

727

728

729

4. Conclusions

730

731

732   This article summarized the advanced photocatalysis mediated by composite $TiO_2/Ag/TiO_2$
733 NPs deposited on cotton fabric using a simple bottom-up synthetic approach. The synthesized
734 $CO+TiO_2/Ag/TiO_2$ nanocomposite with improved photocatalytic performances has been proven
735 to be an efficient and reuse-suitable system for wastewater treatment.

736   The redshift of the SPR band in the UV/Vis absorption spectra of stable TiO_2/Ag NPs (d ~ 8
737 nm), observed by increasing the illumination time, was a consequence of the enlarged sizes of
738 TiO_2/Ag NPs i.e. increased amount of Ag. The uniform distribution of deposited TiO_2/Ag and
739 $TiO_2/Ag/TiO_2$ NPs (d ~ 10 nm) on the cotton fabric was confirmed by FESEM and EDX
740 measurements, whereas the total content of Ti and Ag was 0.47 and 0.06 for $CO+TiO_2/Ag$ and
741 4.90 and 0.01 for $CO+TiO_2/Ag/TiO_2$, respectively. The successful fabrication of Ag NPs on the
742 surface of cotton fabric modified with TiO_2 NPs was confirmed in the diffuse reflectance spectra
743 of the nanocomposites. Raman spectroscopy clearly established the formation of TiO_2 anatase
744 single crystals and provided evidence of a higher amount of TiO_2 NPs deposition in the TiO_2
745 double-loaded sample, which was fully consistent with ICP - OES analysis. Results obtained from
746 the XRD measurements showed the presence of anatase crystalline structure of TiO_2 NPs with low
747 domain of crystallinity and face centred cubic structure of Ag NPs.

748   The exceptional photocatalytic ability, systematically examined for Rhodamine B, Acid
749 Orange 7 and Methyl Red, was achieved with the $CO+TiO_2/Ag/TiO_2$ nanocomposite (> 90%).
750 Respecting the recyclability (three cycles), the mentioned trend was retained, highlighting the
751 significance of TiO_2 NPs double-layer modification over its single processing. In the
752 $TiO_2/Ag/TiO_2$ double-layer processed sample the double quantity of TiO_2 exceeded the threshold
753 necessary to further improve the photocatalytic performances by contributing additional binding
754 sites for dye molecules. Since the photocatalytic activity of the $CO+TiO_2/Ag$ and $CO+TiO_2$
755 samples was practically imperceptible, it can be assumed that the synthesized Ag NPs act
756 predominantly as electron traps in double-loaded research system. The divergent chemical
757 structures of the dyes implied differences in the efficiency of photocatalysis when the same
758 samples were used.

759

Author contributions

Investigation, data curation, visualization, writing – original draft MM, conceptualization, validation, writing – review & editing MR, resources, writing, review SO, resources, writing, review HA, writing, review JS, writing, review LM, Writing – review & editing, Supervision ZŠ.

Funding

Declarations

Conflict of interest

The authors have no conflicts of interest to declare that are relevant to the content of this article.

Ethical approval

This article does not contain any studies with human participants or animals performed by any of the authors.

Consent to participate

All authors have participated in the writing of the manuscript and given their consent to submit the manuscript.

Consent for publication

All authors consent to the publication of the manuscript. consent was obtained from all individual participants included in the study.

814 *References*
815

816 Abid M, Bouattour S, Ferraria AM, Conceição DS, Carapeto AP, Vieira Ferreira LF, Botelho do Rego AM,
817 Chehimi MM, Rei Vilar M, Boufi S (2017) Facile functionalization of cotton with nanostructured
818 silver/titania for visible-light plasmonic photocatalysis. J. Colloid Interface Sci. 507:83-94.
819 https://doi.org/10.1016/j.jcis.2017.07.109

820

821 Agarwal UP, Reiner RS, Ralph SA (2009) Determination of Cellulose | Crystallinity by FT-Raman
822 Spectroscopy. In Proceeding of the 15th International Symposium on Wood, Fiber, and Pulping Chemistry:
823 Oslo, Norway (June 15-18, 2009), Paper No. P-053_ISWFPC_Cellulose_Crystallinity.

824

825 Anwer H, Mahmood A, Lee J, Kim K-H, Park J-W, Yip ACK (2019) Photocatalysts for degradation of
826 dyes in industrial effluents: Opportunities and challenges. Nano. Res. 12:955-972.
827 https://doi.org/10.1007/s12274-019-2287-0

828

829 Bauer C, Jacques P, Kalt A (1999) Investigation of the interaction between a sulfonated azo dye (AO7) and
830 a TiO_2 surface. Chem. Phys. Lett. 307:397-406. https://doi.org/10.1016/S0009-2614(99)00518-7

831

832 Bourikas K, Stylidi M, Kondarides DI, Verykios XE (2005) Adsorption of Acid Orange 7 on the surface of
833 titanium dioxide. Langmuir 21:9222-9230. https://doi.org/10.1021/la051434g

834

835 Cabrales L, Abidi N, Manciu F (2014) Characterization of developing cotton fibers by confocal Raman
836 microscopy. Fibers 2:285-294. https://doi.org/10.3390/fib2040285

837

838 Chakraborty JN (2014) 2 - Colouring materials, Fundamentals and Practices in Colouration of Textiles.
839 Woodhead Publishing India, New Delhi. https://doi.org/10.1016/C2014-0-03947-0

840

841 Chequer FMD, de Oliveira GAR, Ferraz ERA, Cardoso JC, Zanoni MVB, de Oliveira DP (2013) Textile
842 Dyes: Dyeing Process and Environmental Impact. In: Günay M (ed) Eco-Friendly Textile Dyeing and
843 Finishing, IntechOpen, London, pp 151-176. https://doi.org/10.5772/53659

844

845 Chiarello GL, Aguirre MH, Selli E (2010) Hydrogen production by photocatalytic steam reforming of
846 methanol on noble metal-modified TiO_2. J. Catal. 273:182-190. https://doi.org/10.1016/j.jcat.2010.05.012

847

848 Choi HC, Jung YM, Kim SB (2005) Size effects in the Raman spectra of TiO_2 nanoparticles. Vib. Spectrosc.
849 37:33-38. https://doi.org/10.1016/j.vibspec.2004.05.006

850

851 Dastjerdi R, Montazer M (2010) A review on the application of inorganic nano-structured materials in the
852 modification of textiles: Focus on anti-microbial properties. Colloids Surf. B 79:5-18.
853 https://doi.org/10.1016/j.colsurfb.2010.03.029

854

855 Eronen P, Österberg M, Jääskeläinen A-S (2009) Effect of alkaline treatment on cellulose supramolecular
856 structure studied with combined confocal Raman spectroscopy and atomic force microscopy. Cellulose
857 16:167-178. https://doi.org/10.1007/s10570-008-9259-8

858

Fan Y, Chen G, Li D, Luo Y, Lock N, Jensen AP, Mamakhel A, Mi J, Iversen SB, Meng Q, Iversen BB (2012) Highly selective deethylation of rhodamine B on TiO_2 prepared in supercritical fluids. Int. J. Photoenergy 2012, Article ID 173865. https://doi.org/10.1155/2012/173865

Ghime D, Ghosh P (2020) Advanced Oxidation Processes: A Powerful Treatment Option for the Removal of Recalcitrant Organic Compounds. In: Bustillo-Lecompte C (ed) Advanced Oxidation Processes - Applications, Trends, and Prospects, IntechOpen, London, pp 3-14. https://doi.org/10.5772/intechopen.90192

Goddard III WA, Brenner D, Lyshevski SE, Iafrate GJ (2012) Handbook of Nanoscience, Engineering, and Technology, 3rd edn. CRC Press, Boca Raton. https://doi.org/10.1201/9781315217178

Julkapli NM, Bagheri S, Hamid SBA (2014) Recent advances in heterogeneous photocatalytic decolorization of synthetic dyes. Sci. World J. 2014, Article ID 692307. https://doi.org/10.1155/2014/692307

Kamat PV (2002) Photophysical, photochemical and photocatalytic aspects of metal nanoparticles. J. Phys. Chem. B 106:7729-7744. https://doi.org/10.1021/jp0209289

Kapilashrami M, Zhang Y, Liu Y-S, Hagfeldt A, Guo J (2014) Probing the Optical Property and Electronic Structure of TiO_2 Nanomaterials for Renewable Energy Applications. Chem. Rev. 114:9662-9707. https://doi.org/10.1021/cr5000893

Keshk M.A.S, Hamdy M.S. (2019) Preparation and physicochemical characterization of zinc oxide/sodium cellulose composite for food packaging. Turk J Chem 43: 94 – 105. https://doi.org/10.3906/kim-1803-83

Khataee AR, Kasiri MB (2010) Photocatalytic degradation of organic dyes in the presence of nanostructured titanium dioxide: Influence of the chemical structure of dyes. J Mol Catal A Chem 328:8-26. https://doi.org/10.1016/j.molcata.2010.05.023

Kochuveedu ST, Jang YH, Kim DH (2013) A study on the mechanism for the interaction of light with noble metal-metal oxide semiconductor nanostructures for various photophysical applications. Chem. Soc. Rev. 42:8467-8493. https://doi.org/10.1039/C3CS60043B

Kuball HG, Höfer T, Kiesewalter S (2017) Chiroptical Spectroscopy, General Theory. In: Lindon JC, Tranter GE, Koppenaal DW (eds-in-chief) Encyclopedia of Spectroscopy and Spectrometry, 3rd edn. Academic Press Massachusetts, Cambridge, pp 217-231. https://doi.org/10.1016/B978-0-12-409547-2.04980-5

Lellis B, Fávaro-Polonio CZ, Pamphile JA, Polonio JC (2019) Effects of textile dyes on health and the environment and bioremediation potential of living organisms. Biotechnol. Res. Innov. 3:275-290. https://doi.org/10.1016/j.biori.2019.09.001

Leong KH, Gan BL, Ibrahim S, Saravanan P (2014) Synthesis of surface plasmon resonance (SPR) triggered Ag/TiO_2 photocatalyst for degradation of endocrine disturbing compounds. Appl. Surf. Sci. 319:128-135. https://doi.org/10.1016/j.apsusc.2014.06.153

904

905 Linsebigler AL, Lu G, Yates JT (1995) Photocatalysis on TiO$_2$ Surfaces: Principles, Mechanisms, and
906 Selected Results. Chem. Rev. 95:735-758. https://doi.org/10.1021/cr00035a013

907

908 Liu Y, Kokot S, Sambi TJ (1998) Vibrational spectroscopic investigation of Australian cotton cellulose
909 fibres: Part 1. A Fourier transform Raman study. Analyst 123:633-636. https://doi.org/10.1039/A707064K

910

911 Ma Y, Yao J-N (1998) Photodegradation of Rhodamine B catalyzed by TiO$_2$ thin films. J. Photochem.
912 Photobiol. A 116:167-170. https://doi.org/10.1016/S1010-6030(98)00295-0

913

914 Marković D, Šaponjić Z, Radoičić M, Radetić T, Vodnik V, Potkonjak B, Radetić M (2015)
915 Sonophotocatalytic degradation of dye C.I. Acid Orange 7 by TiO$_2$ and Ag nanoparticles immobilized on
916 corona pretreated polypropylene non-woven fabric. Ultrason Sonochem 24:221-229.
917 https://doi.org/10.1016/j.ultsonch.2014.11.017

918

919 Meng Y (2015) A Sustainable Approach to Fabricating Ag Nanoparticles/PVA Hybrid Nanofiber and Its
920 Catalytic Activity. Nanomaterials 5:1124-1135 https://doi.org/10.3390/nano5021124

921

922 Mihailović D, Šaponjić Z, Vodnik V, Potkonjak B, Jovančić P, Nedeljković JM, Radetić M (2011)
923 Multifunctional PES fabrics modified with colloidal Ag and TiO$_2$ nanoparticles. Polym Adv Technol
924 22:2244-2249. https://doi.org/10.1002/pat.1752

925

926 Milošević M, Radoičić M, Šaponjić Z, Nunney T, Marković D, Nedeljković J, Radetić M (2013) In situ
927 generation of Ag nanoparticles on polyester fabrics by photoreduction using TiO$_2$ nanoparticles.
928 J. Mater. Sci. 48:5447 - 5455. https://doi.org/10.1007/s10853-013-7338-1

929

930 Milošević M, Radoičić M, Šaponjić Z, Nunney T, Deeks C, Lazić V, Mitrić M, Radetić T, Radetić M (2014)
931 In situ photoreduction of Ag$^+$-ions by TiO$_2$ nanoparticles deposited on cotton and cotton/PET fabrics.
932 Cellulose 21:3781 - 3795. https://doi.org/10.1007/s10570-014-0373-5

933

934 Milošević M, Šaponjić Z, Nunney T, Deeks C, Radoičić M, Mitrić M, Radetić T, Radetić M (2017) In situ
935 photoreduction of Ag$^+$-ions on the surface of titania nanotubes deposited on cotton and cotton/PET fabrics.
936 Cellulose 24:1597-1610. https://doi.org/10.1007/s10570-017-1207-z

937

938 Montazer M, Behzadnia A, Pakdel E, Rahimi MK, Moghadam MB (2011) Photo induced silver on nano
939 titanium dioxide as an enhanced antimicrobial agent for wool. J. Photochem. Photobiol. B, Biol. 103:207-
940 214. https://doi.org/10.1016/j.jphotobiol.2011.03.009

941

942 Morones JR, Elechiguerra JL, Camacho A, Holt K, Kouri JB, Ramírez JT, Yacaman MJ (2005) The
943 bactericidal effect of silver nanoparticles. Nanotechnology 16:2346-2353.
944 https://doi.org/10.1088/0957-4484/16/10/059

945

946 Ohsaka T, Izumi F, Fujiki Y (1978) Raman spectrum of anatase, TiO$_2$. J Raman Spectrosc 7:321-324.
947 https://doi.org/10.1002/jrs.1250070606

948

949   Ohsaka T (1980) Temperature dependence of the Raman spectrum in anatase TiO_2. J. Phys. Soc. Jpn.
950   48:1661-1668. https://doi.org/10.1143/JPSJ.48.1661

951
952   Park H, Choi W (2005) Photocatalytic reactivities of Nafion-coated TiO_2 for the degradation of charged
953   organic compounds under UV or visible light. J. Phys. Chem. B 109:11667-11674.
954   https://doi.org/10.1021/jp051222s

955
956   Radetić M (2013a) Functionalization of textile materials with TiO_2 nanoparticles. J. Photochem. Photobiol.
957   C 16:62-76. https://doi.org/10.1016/j.jphotochemrev.2013.04.002

958
959   Radetić M (2013b) Functionalization of textile materials with silver nanoparticles. J. Mater. Sci. 48:95-107.
960   https://doi.org/10.1007/s10853-012-6677-7

961
962   Radoičić M, Ćirić-Marjanović G, Spasojević V, Ahrenkiel P, Mitrić M, Novaković T, Šaponjić Z (2017)
963   Superior photocatalytic properties of carbonized PANI/TiO_2 nanocomposites. Appl. Catal. B 213:155-166.
964   https://doi.org/10.1016/j.apcatb.2017.05.023

965
966   Rajh T, Nedeljković J, Chen LX, Tiede DM, Thurnauer MC (1998) Photoreduction of copper on TiO2
967   nanoparticles modified with polydentate ligands. J. Adv. Oxid. Technol. 3:292-298.
968   https://doi.org/10.1515/jaots-1998-0314

969
970   Rashid MM, Tomšič B, Simončič B, Jerman I, Štular D, Zorc M (2022) Sustainable and cost-effective
971   functionalization of textile surfaces with Ag-doped TiO_2/polysiloxane hybrid nanocomposite for UV
972   protection, antibacterial and self-cleaning properties. Appl. Surf. Sci. 595, Article ID 153521.
973   https://doi.org/10.1016/j.apsusc.2022.153521

974
975   Reza KM, Kurny A, Gulshan F (2017) Parameters affecting the photocatalytic degradation of dyes using
976   TiO_2: a review. Appl. Water Sci. 7:1569-1578. https://doi.org/10.1007/s13201-015-0367-y

977
978   Rivero PJ, Urrutia A, Goicoechea J, Arregui FJ (2015) Nanomaterials for functional textiles and fibers.
979   Nanoscale Res. Lett. 10, Article ID 501. https://doi.org/10.1186/s11671-015-1195-6

980
981   Rupa AV, Manikandan D, Divakar D, Sivakumar T (2007) Effect of deposition of Ag on TiO_2 nanoparticles
982   on the photodegradation of Reactive Yellow-17. J. Hazard. Mater. 147:906-913.
983   https://doi.org/10.1016/j.jhazmat.2007.01.107
984   Schenzel K, Fischer S, Brendler E (2005) New method for determining the degree of cellulose | Crystallinity
985   by means of FT Raman spectroscopy. Cellulose 12:223-231. https://doi.org/10.1007/s10570-004-3885-6

986
987   Schmid G (2004) Nanoparticles: From Theory to Application. Wiley-VCH Verlag GmbH & Co. KGaA,
988   Weinheim. https://doi.org/10.1021/ja040954f

989
990   Schneider J, Matsuoka M, Takeuchi M, Zhang J, Horiuchi Y, Anpo M, Bahnemann DW (2014)
991   Understanding TiO_2 Photocatalysis: Mechanisms and Materials. Chem. Rev. 114:9919-9986.
992   https://doi.org/10.1021/cr5001892

993

994 Sousa-Castillo A, Comesaña-Hermo M, Rodriguez-Gonzalez B, Pérez-Lorenzo M, Wang Z, Kong X-T,
995 Govorov AO, Correa-Duarte MA (2016) Boosting Hot Electron-Driven Photocatalysis through Anisotropic
996 Plasmonic Nanoparticles with Hot Spots in Au-TiO$_2$ Nanoarchitectures. J. Phys. Chem. C 120:11690-
997 11699. https://doi.org/10.1021/acs.jpcc.6b02370

999 Szabó-Bárdos E, Czili H, Horváth A (2003) Photocatalytic oxidation of oxalic acid enhanced by silver
1000 deposition on a TiO$_2$ surface. J. Photochem. Photobiol. A 154:195-201.
1001 https://doi.org/10.1016/S1010-6030(02)00330-1

1003 Wang Q, Chen C, Zhao D, Ma W, Zhao J (2008) Change of adsorption modes of dyes on fluorinated TiO$_2$
1004 and its effect on photocatalytic degradation of dyes under visible irradiation. Langmuir 24:7338-7345.
1005 https://doi.org/10.1021/la800313s

1007 Watanabe T, Takizawa T, Honda K (1977) Photocatalysis through excitation of adsorbates. 1. Highly
1008 efficient N-deethylation of rhodamine B adsorbed to cadmium sulphide. J. Phys. Chem. 81:1845-1851.
1009 https://doi.org/10.1021/j100534a012

1011 Wiley JH, Atalla RH (1987) Band assignments in the Raman spectra of celluloses. Carbohydr. Res.
1012 160:113-129. https://doi.org/10.1016/0008-6215(87)80306-3

1014 Xiao M, Jiang R, Wang F, Fang C, Wang J, Yu JC (2013) Plasmon-enhanced chemical reactions. J. Mater.
1015 Chem. A 1:5790-5805. https://doi.org/10.1039/C3TA01450A
1016

1017 Yaseen DA, Scholz M (2019) Textile dye wastewater characteristics and constituents of synthetic effluents:
1018 a critical review. Int. J. Environ. Sci. Technol. 16:1193-1226. https://doi.org/10.1007/s13762-018-2130-z

1020 Yu K, Yang S, He H, Sun C, Gu C, Ju Y (2009) Visible light-driven photocatalytic degradation of
1021 rhodamine B over NaBiO$_3$: Pathways and mechanism. J. Phys. Chem. A 113:10024-10032.
1022 https://doi.org/10.1021/jp905173e

1024 Zhang X, Jin M, Liu Z, Tryk DA, Nishimoto S, Murakami T, Fujishima A (2007) Superhydrophobic TiO$_2$
1025 surfaces: Preparation, photocatalytic wettability conversion, and superhydrophobic-superhydrophilic
1026 patterning. J. Phys. Chem. C 111:14521-14529. https://doi.org/10.1021/jp0744432

1030 **Figure Captions**

1032 **Fig. 1.** TEM micrographs of colloidal TiO$_2$ (a) and TiO$_2$/Ag NPs (b) and the appropriate particle size
1033 distributions (c and d).

1034 **Fig. 2.** Absorption spectra of TiO$_2$/Ag NPs colloidal dispersion for different illumination times.

1035 **Fig. 3.** FESEM micrographs of cotton fiber (CO control) and cotton fibers coated with TiO$_2$/Ag.

1036 and TiO$_2$/Ag/TiO$_2$ NPs along with their respective EDX spectra.

1037 **Fig. 4.** Raman spectra of the CO+TiO$_2$, CO+TiO$_2$/Ag and CO+TiO$_2$/Ag/TiO$_2$ samples.

1038 **Fig. 5.** Diffuse reflectance spectra of the CO control, CO+TiO$_2$/Ag and CO+TiO$_2$/Ag/TiO$_2$ samples.

1039 **Fig. 6.** Photodegradation curves (C/C0) of Rhodamine B for the tested samples (a), absorption spectra of
1040 Rhodamine B (554 nm) to Rhodamine (497 nm) blue-shift transition for CO+TiO$_2$/Ag sample (b), N-
1041 deethylation process of Rhodamine B to Rhodamine (Schmid 2004) (c) and suitable wavelengths changes
1042 during the photocatalysis of Rhodamine B (d).

1043 **Fig. 7.** Photodegradation curves (C/C0) of Acid Orange 7 for the tested samples (a), chemical structure of
1044 Acid Orange 7 (b).

1045 **Fig. 8.** Photodegradation curves (C/C0) of Methyl Red for the tested samples (a), chemical structure of
1046 Methyl Red (b).

1047 **Fig. 9.** Photoinduced charge separation in TiO$_2$/Ag/TiO$_2$-mediated photodegradation system (UV light) -
1048 Mechanism 1 (a) photochemical processes on the surface of the synthesized nanocomposite induced by
1049 visible light - Mechanism 2 (b) TiO$_2$/Ag/TiO$_2$ NPs modified cotton fabric composite (c).
1050
1051 **Fig. 10.** The images of aliquots at specific time intervals for the tested samples and dyes.

1052 **Fig. 11.** The images of the tested samples before and after photocatalysis.

1053 **Fig. 12.** Photocatalytic efficiency of the CO+TiO$_2$ (a), CO+TiO$_2$/Ag (b) and CO+TiO$_2$/Ag/TiO$_2$ (c)
1054 samples after three reuse cycles (illumination time: 300 min for RB and AO7, 120 min for MR).

1055 **Table 1.** Surface elemental composition of nanocomposites based on EDX analysis.

1056 **Table 2.** Photocatalytic degradation of Rhodamine B, Acid Orange 7 and Methyl Red.